

Predictive Mobility and Location-Aware Routing Protocol in
Mobile Ad Hoc Networks

Student : Tse-En Lu

Advisor : Kai-Ten Feng

Department of Communication Engineering

National Chiao Tung University

October 12, 2005

Abstract

Many Location-aware routing protocols have been proposed for the mobile ad hoc networks in recent years. The efficiency of the routing protocols can be improved by considering the location information of the mobile nodes. However, the mobility characteristics of the mobile node have not been taken into account in most of the related work. In this thesis, the proposed Velocity Aided Routing (VAR) protocol determines its packet forwarding scheme based on the relative velocity between the intended forwarding node and the destination node. The routing performance can be further improved by the proposed Predictive Mobility and Location-Aware Routing (PMLAR) algorithm, which incorporates the predictive moving behaviors of the mobile nodes in the protocol design. The region for packet forwarding is determined by predicting the future trajectory of the destination node. The routing performance can be effectively improved by adopting the prediction mechanism of the proposed PMLAR algorithm. Simulation results show that the PMLAR protocol and its derivative algorithms outperform other routing protocols under different network topologies.

Contents

1	Introduction	3
2	Key Components and Related Work in MANET	6
2.1	Physical Layer	7
2.1.1	Propagation Models	7
2.1.2	Physical Transmission	8
2.2	MAC Layer	10
2.2.1	Distributed Coordination Function	10
2.2.2	Hidden Node Problem	12
2.2.3	Exposed Terminal Problem	12
2.3	Network Layer	14
2.3.1	Existing Ad-Hoc Routing Protocols	14
2.3.2	The Dynamic Source Routing (DSR) Protocol	15
2.3.3	The Location-Aided Routing (LAR) Protocol	17
3	Mobility Models	20
3.1	The Gauss-Markov Mobility (GMM) Model	20
3.1.1	Parameter Estimation of the Gauss-Markov Mobility Model	22
3.2	The Constant Speed Mobility (CSM) Model	24
3.3	The Random Waypoint Mobility (RWM) Model	26
3.4	The Highway Mobility (HM) Model	26

4	The Proposed Mobility and Location-Based Routing Protocols	30
4.1	The Velocity Aided Routing (VAR) Protocol	32
4.1.1	The VAR using the Gauss-Markov Mobility Model (VAR-GMM)	33
4.1.2	The VAR using the Constant Speed Mobility Model (VAR-CSM)	35
4.2	The Predictive Mobility and Location-Aware Routing (PMLAR) Protocol	36
4.2.1	The PMLAR Protocol	36
4.2.2	The PMLAR Protocol with VAR Algorithm (PMLAR-V)	41
5	Performance Evaluation	43
5.1	Parameter Estimation	43
5.1.1	Parameter Estimation of RWM Model	43
5.1.2	Parameter Estimation of RWM Model under Different Simulation Models	45
5.1.3	Parameter Estimation of HM Model	46
5.1.4	Parameter Estimation of HM Model under Different Simulation Models	49
5.2	Simulation Results	50
5.2.1	Simulation Parameters	50
5.2.2	Simulation Results of the VAR Protocol	51
5.2.3	Simulation Results of the PMLAR Protocol	51
6	Conclusions	57

Chapter 1

Introduction

A Mobile Ad hoc NETWORK (MANET) consists of wireless Mobile Nodes (MNs) that cooperatively communicate with each other without the existence of fixed network infrastructure. Fig. 1.1 shows the framework of wireless ad hoc network, where each MN communicates with others not via infrastructure but the peers. Depending on different geographical topologies, the MNs are dynamically located and continuously changing their locations. The fast-changing characteristics in MANETs make it difficult to discover routes between MNs. It becomes important to design efficient and reliable routing protocols to maintain, discover, and organize the routes in MANETs.

The concepts of MANET began at 1970s. One of the original motivations is to satisfy the requirement of high mobility and reliability military communication system. In such severe battle environment, the communication devices can not rely on the pre-installed communication infrastructures because they may not exist or they can be destroyed immediately. In another word, the military wireless communication system is different from general commercial system in the situation where the flexibility, mobility, and reliability are needed. The tactical information and managerial message are transmitted in the unpredictable battle, which are the major factors why the military communication needs MANET. The MANET is not only used in military communication but can also be applied generally in Inter-Vehicle Communication (IVC), message delivery, disasters recovery, sensor network, the Personal Communication

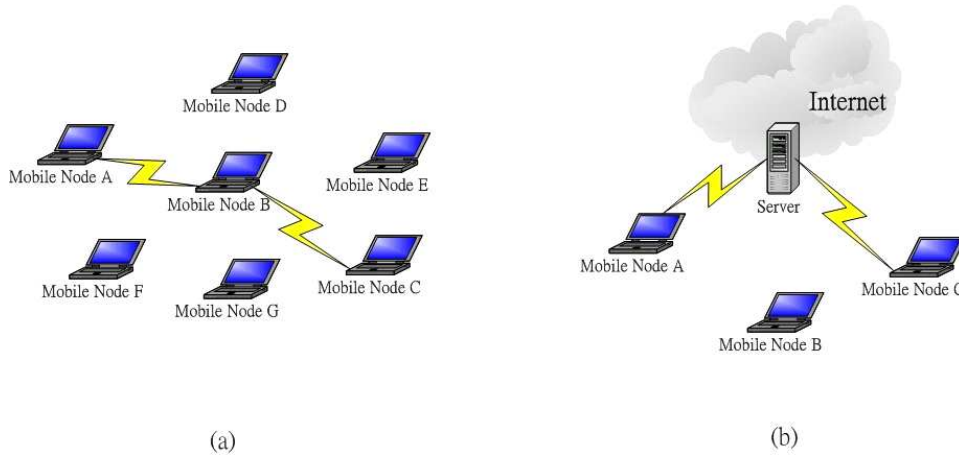


Figure 1.1: (a)Ad hoc network: node A communicate with node C via mobile node B
 (b)Infrastructure network: node A communicate with node C via infrastructure

Services (PCSs), and educational purpose. There are two examples of MANET described as follows:

- **The Intelligent Transportation System (ITS):** With the capability of self-organizing, the MANET provides the wireless communication routes between vehicles. This capability is also useful when emergencies happen in rural area because it will be much easier to communicate with police using MANET. Similarly, the MANET can help to save lives in mountains or in seas which have no expected network infrastructure provided. In the limited space and time, the MANET is especially satisfactory because of its wireless and movable features.
- **The Personal Communication Service (PCS):** As the personal communication devices are becoming more powerful, the related technology is required to deal with mass data transmission, including computer files exchange and exhibition of application programs. The MANET can provide data transmission efficiently by forming a temporary network topology instead of a large infrastructure or a point-to-point transmission line.

In this thesis, the Velocity Aided Routing (VAR) and Predictive Mobility and Location-Aided Routing (PMLAR) algorithms are proposed by further considering the motion behavior of MNs to provide efficient routing performance. The proposed Velocity Aided Routing

(VAR) algorithm determines its packet forwarding scheme by calculating the relative velocity between the potential forwarding nodes and the destination node. This scheme forwards the data packets via those intermediate nodes that are faster approaching the destination node. The Gauss-Markov Mobility (GMM) Model [34] [35] and the Constant Speed Mobility (CSM) Model are utilized in the design of the VAR algorithm to compute the MN's speed and moving angle. Moreover, since mobility of the MNs diverse under different moving scenarios, it will be beneficial to incorporated the MN's predicted movement in the design of routing protocols. The proposed Predictive Mobility and Location-Aware Routing (PMLAR) algorithm determines its packet forwarding scheme by predicting the current and the future position of the destination node. The prediction mechanism defines the packet forwarding region by adapting its adjustable parameters based on the previous moving behavior of the destination node. The GMM model is also utilized in the design of the PMLAR algorithm.

The remainder of this thesis is organized as follows. Chapter 2 introduces the key components and related work of MANET in the physical, Medium Access Control (MAC), and network layers. The four mobility models, the Gauss-Markov Mobility (GMM), the Constant Speed Mobility (CSM), the Random Waypoint Mobility (RWM), and the Highway Mobility (HM) models, are presented in chapter 3. Chapter 4.1 shows the proposed Velocity Aided Routing (VAR) protocol based on GMM and CSM predictive mobility models. The proposed Predictive Mobility and Location-Aware Routing protocol and its derivative algorithms are presented in chapter 4.2. The estimation of parameters and the performance evaluation of the proposed routing protocols are shown chapter in 5.1 and 5.2. Chapter 6 draws the conclusions.

Chapter 2

Key Components and Related Work in MANET

In this section, the key components which enable the communication between mobile ad hoc nodes will be presented. According to the structure of Open System Interconnect (OSI), the key communication layers that we are interested in the ad hoc field includes the physical layer, the MAC layer, and the network routing layer. Depending on these layers, many ad hoc applications can be developed and executed as shown in Fig. 2.1. In the physical layer, the radio propagation model are utilized to formulate the radio phenomenon and the baseband system achieves the data transmission between MNs. How nodes share the same medium is also an important issue in wireless system, which will be introduced in MAC layer. By considering the transmission range, data rate, and popularity, the IEEE 802.11 wireless local area network (WLAN) is the most suitable for mobile ad hoc networks. Our discussion will focus on the specification of IEEE 802.11. Finally, several ad hoc routing protocols will be studied in network layer.

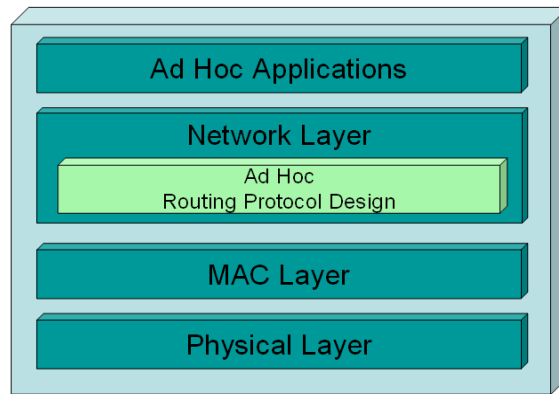
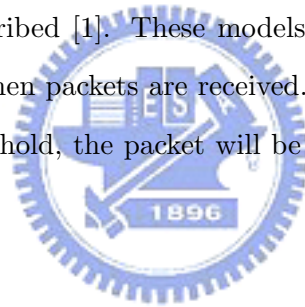


Figure 2.1: Communication stacks of the mobile ad hoc applications

2.1 Physical Layer

2.1.1 Propagation Models

In this section, three radio propagation models including free space, two-ray ground reflection, and shadowing model are described [1]. These models can be used to predict the received signal power at receiver side when packets are received. If received power of packet is below the threshold that the receiver hold, the packet will be regarded as error and is drop by the MAC layer.



Free Space Model

There is only one line-of-sight path between transmitter and receiver in the assumption of free space model. The received power with distance d can be calculated as:

$$P_r(d) = \frac{P_t G_t G_r \lambda^2}{(4\pi)^2 d^2 L} \quad (2.1)$$

where P_t is the transmitted signal power, G_t and G_r are the antenna gains of the transmitter and the receiver respectively, L is the system loss, and λ is the wavelength.

Two-Ray Ground Reflection Model

The two-ray ground model considers both line-of-sight path and reflected path by ground between transmitter and receiver. The received power can be predicted as:

$$P_r(d) = \frac{P_t G_t G_r h_t^2 h_r^2}{d^4 L} \quad (2.2)$$

where h_t and h_r are the heights of the transmit and receive antennas.

The two-ray ground model provides more accurate predicted power than the free space model at long distance scenario; while the free space model outperforms the two-ray ground model at short distance. In order to decide which models should be utilized, the threshold d_{th} is determined by:

$$d_{th} = \frac{(4\pi h_t h_r)}{\lambda} \quad (2.3)$$

In the case when $d < d_{th}$, Eqn (2.1) is used; otherwise, Eqn (2.2) is adopted.

Shadowing Model

A more realistic model called Shadowing Model considers the fading effect to predicted the received power as a non-ideal circle. The following equation represents the shadowing model at a distance d :

$$\left[\frac{P_r(d)}{P_r(d_0)} \right]_{dB} = -10\beta \log \frac{d}{d_0} + X_{dB} \quad (2.4)$$

where $P_r(d_0)$ can be obtained from Eqn (2.1); β is path loss exponent; and X_{dB} is a Gaussian random variable with zero mean and standard deviation σ_{dB} .

2.1.2 Physical Transmission

The IEEE 802.11 [2] denotes a set of Wireless LAN standards developed by working group 11 of the IEEE LAN/MAN Standards Committee. The term also used to refer as the original

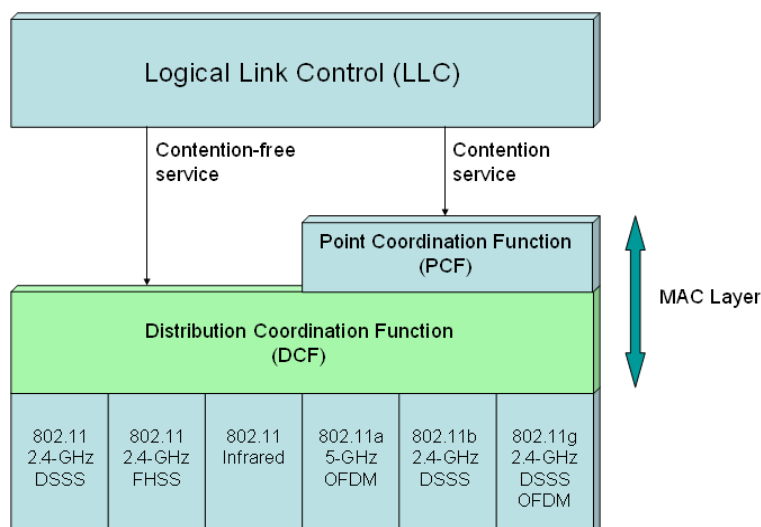


Figure 2.2: IEEE 802.11 protocol architecture

802.11, which is now called "802.11 legacy". The most popular techniques in the 802.11 family are those defined by the a, b, and g amendments to the original standard. Fig. 2.2 shows the IEEE 802.11 protocol architecture. The original version of the standard IEEE 802.11 is released in 1997. It specifies two raw data rates of 1 and 2 Mbps and transmits via infrared (IR) signals or in the ISM band at 2.4 GHz. The Carrier Sense Multiple Access with Collision Avoidance (CSMA/CA) are defined as the media access method which will be studied in next section.

The 802.11b amendment to the original standard was approved in 1999. By directly extending the DSSS modulation technique defined in the original 802.11 standard, 802.11b can operate at 11Mbps but will scale back to 5.5, 2, and 1 Mbps if signal quality becomes an issue. The 802.11a amendment to the original standard was approved in 1999, which is non-interoperable with 802.11b, except for equipment that implements both standards. The 802.11a operates in 5 GHz band and uses a 52-subcarrier Orthogonal Frequency Division Multiplexing (OFDM) with a maximum raw data rate of 54 Mbps. The data rate can be reduced to 48, 36, 34, 18, 9, and 6 Mbps if required. The 802.11g amendment was approved in June 2003. It works in the 2.4 GHz band (like 802.11b) but operates at a maximum raw data rate of 54Mbps, or about 24.7 Mbps net throughput like 802.11a.

2.2 MAC Layer

In this section, the mechanisms of IEEE 802.11 Medium Access Control (MAC) [2] are described. The MAC provides several services including data exchange, power-control, and synchronization. It is also responsible for interpreting the received bit stream from physical layer to network layer.

2.2.1 Distributed Coordination Function

The Distributed Coordination Function (DCF) is a basic access mechanism utilized by the MAC protocol in IEEE 802.11. The DCF is based on a Carrier Sense Multiple Access (CSMA) with Collision Avoidance (CA) which guarantees each station a fair chance to access the medium. By using CSMA/CA, each node has to sense the medium before data transmission. If the medium is found idle, the data is allowed to send. In order to avoid collision, the station selects a random backoff time slots and freezes transmission until the time slot decreasing to zero. The MANET is a self-organized network without centralized node to control the usage of medium. The IEEE 802.11 DCF is a simple and fair mechanism that satisfies the requirement of MANET.

However, the fast changing characteristic of wireless medium makes the correct operation of carrier sense a difficult problem. The IEEE 802.11 MAC protocol provides additional mean called virtual carrier sensing as a backup mechanism to avoid collisions. Virtual carrier sensing is carried out by NAV (Network Allocation Vector) which records the duration of ongoing data transmission. The data can be transmitted only when both physical and virtual carrier sense mechanism detect that the medium is idle.

Before the data transmission, each station executes backoff process to ensure the low probability of collision. As show in Fig. 2.3, the station uniformly selects time slots from $[0, CW]$ which is predefine by IEEE802.11. However, the stations may choose the same time slots under congestion networks. The binary exponential backoff algorithm is executed by using double CW size to avoid the collision again.

The IEEE802.11 MAC defines multiple Inter Frame Space (IFS) which are utilized to

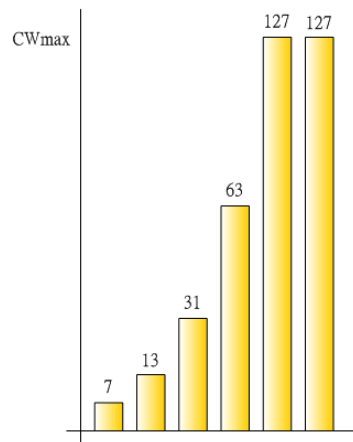


Figure 2.3: Binary exponential backoff algorithm.

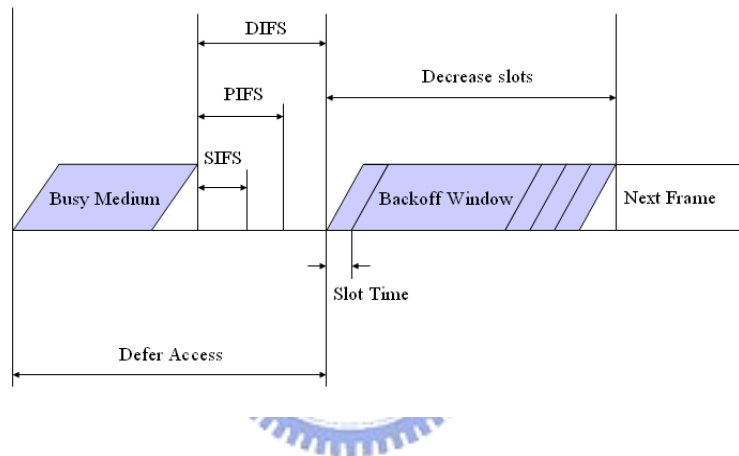


Figure 2.4: The medium access via different Inter Frame Space (IFS).

provide different priorities for medium access including short IFS (SIFS), PCF IFS (PIFS), DCF IFS (DIFS), and Extended IFS (EIFS). As shown in Fig. 2.4, the SIFS is the shortest time spacing with which the station can immediately respond the request like Ack and CTS. The Point Coordinator Function (PCF) is a contention free service and the infrastructure is responsible for monitoring the transmission between each station. To ensure the service being contention free, $DIFS > PIFS$ can avoid the DCF interfering the transmission of PCF. Finally, waiting the largest time spacing EIFS means the packet retransmission (i.e. collision occurs).

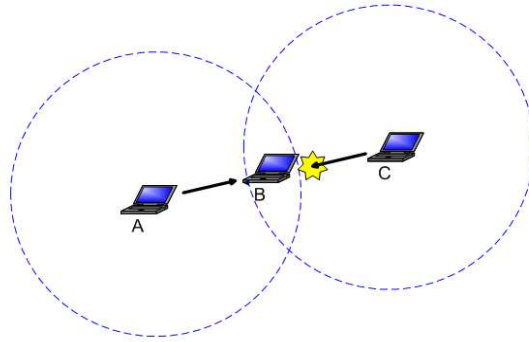


Figure 2.5: Hidden Node Problem

2.2.2 Hidden Node Problem

Due to the limited transmission range, the CSMA can not detect the data transmission that are out of the sense range, which causes the hidden node problem. The hidden node problem will result in the degradation of performance. As shown in Fig. 2.5, the node *A* is transmitting a packet to node *B*. At this moment, the node *C* also initiates a new transmission but the carrier sense can not function since *C* is outside the transmission range of *A*. The collision will occur at *B* and *A* has to retransmit the packet.

The solution of hidden node problem is that each station exchanges smaller packets called RTS and CTS to reserve the channel before data transmission. In Fig. 2.6, *A* send RTS to *B* and *B* replies a CTS to *A*. It is noted that *C* is also informed not to send packet by receiving the CTS.

2.2.3 Exposed Terminal Problem

The RTS/CTS protect the data by blocking the nodes around the transmission pair, which degrade the throughput of network. Fig. 2.7 shows the exposed terminal problem. Because *A* is blocked by the CTS of *B*, *D* can not send its packet to *A* even if this transmission will not affect *B* and *C*.

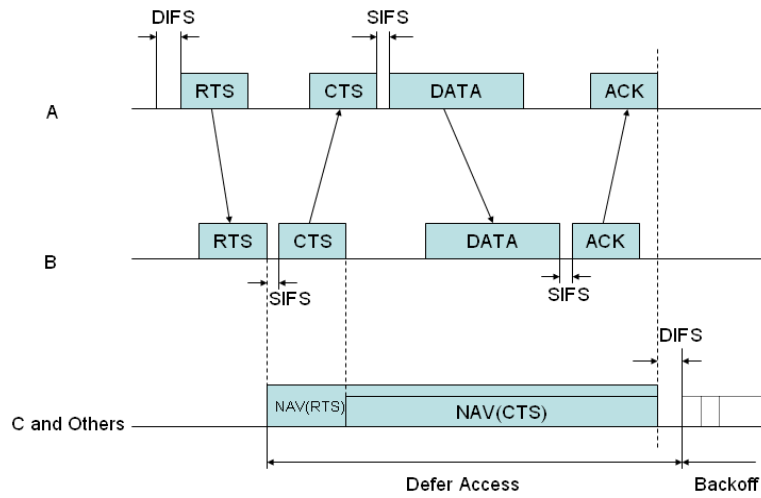


Figure 2.6: Timing diagram of RTS/CTS packet exchange.

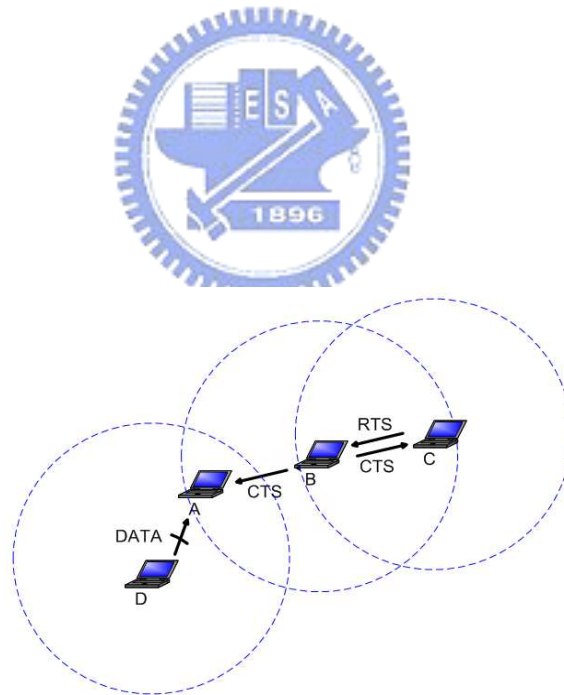


Figure 2.7: Exposed Terminal Problem

2.3 Network Layer

The network layer is responsible for handling the routing problem between the MNs. It discovers, maintains, and terminates the connection of the data transmission. The metrics such as shortest path and power consumption can be taken into consideration for path selection among all possible routes. In this section, we present the existing ad-hoc routing protocols as the background of the proposed algorithms.

2.3.1 Existing Ad-Hoc Routing Protocols

A number of ad hoc routing protocols have been developed for the MANETs. The topology-based routing protocols can be categorized into proactive (such as DSDV [3] and WRP [4]) and reactive algorithms (such as AODV [5], DSR [6], TORA [7], ABR [8], and SSA [9]). The proactive routing protocols periodically maintain tables at each MN. The routing tables records persistent and up-to-date information within the changing network topologies. The proactive algorithms offer reliable routing information between the MNs; while the overheads for maintaining the routing tables can be increased rapidly as the expansion of the MN's numbers and mobility within the network. The reactive algorithms initiate route discovery processes based on the request from the source node. The routing tables are only maintained within the requested routes from the source to the destination nodes. The on-demand characteristics of the reactive algorithms generate less routing overheads comparing with the proactive routing protocols. However, the comparably weak communication linkages and the delay occurred by the route discovery processes make the reactive algorithms less feasible for fast-changing network topologies.

The hybrid routing approaches (such as ZRP [10] [11], CGSR [12] [13], and Cedar [14]) compromise the benefits between the proactive and the reactive algorithms. ZRP utilizes the proactive-based approach within its pre-determined local area; while the reactive algorithm is adopted outside the area. Cluster heads (as in CGSR) or cores (as in Cedar) are selected within the MNs which are served as the gateways for information distribution between the MNs. The hybrid approaches can be utilized to adopted themselves between the communication

reliability and the routing overheads. The performance comparison between various type of ad hoc routing protocols have been conducted in several studies, as in [15]- [18].

There are increasing interests in the design of location-based ad hoc routing algorithms [19]. With the prosperous of mobile devices equipped with positioning systems (such as Global Positioning Systems, GPSs [20]), it becomes feasible to utilize location information from the mobile devices in the routing protocol design (such as DREAM [21], LAR [22], GRA [23], GPSR [24], and GLS [25] [26]). The DREAM protocol proactively distributes the location information of each MN within the network. The data packets are delivered from the source node to the destination node based on the built-in location database within each MN. The LAR protocol, on the other hand, is a reactive location-based algorithm. The route discovery and packet forwarding region is restricted within a pre-determined area based on the knowledge of the MN's location. The routing overhead can be reduced by the restricted directional flooding scheme.

2.3.2 The Dynamic Source Routing (DSR) Protocol

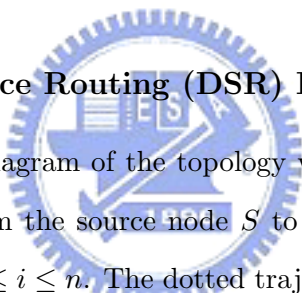


Fig. 2.8 shows the schematic diagram of the topology with the MNs. The data packets are intended to be transmitted from the source node S to the destination node D via some of the forwarding nodes N_i , for $1 \leq i \leq n$. The dotted trajectory indicates the intended routing trajectory of from S to D .

The Dynamic Source Routing (DSR) protocol [6] is a source initiative, on-demand routing algorithm. As shown in Figs. 2.8 and 2.9, The source node S intends to send data packets to the destination node D . S will first check its route cache to verify if there are existing routes to the destination node D . If there is no such route in the cache, S will start a route discovery process by broadcasting a route request ($RREQ_d^{(n)}$) packet at time $t_{r,s}^{(n)}$. The addresses of S and D are both written on the route record in the $RREQ_d^{(n)}$ packet header, i.e. $RREQ_d^{(n)}\langle Adr_S, Adr_D \rangle$. Upon receiving the $RREQ_d^{(n)}$ packet, all the neighborhood MNs, including the forwarding node N_i , will rebroadcast the packet if the route to D is not available. N_i will also add its own address to the route record in the $RREQ_d^{(n)}$ packet in order

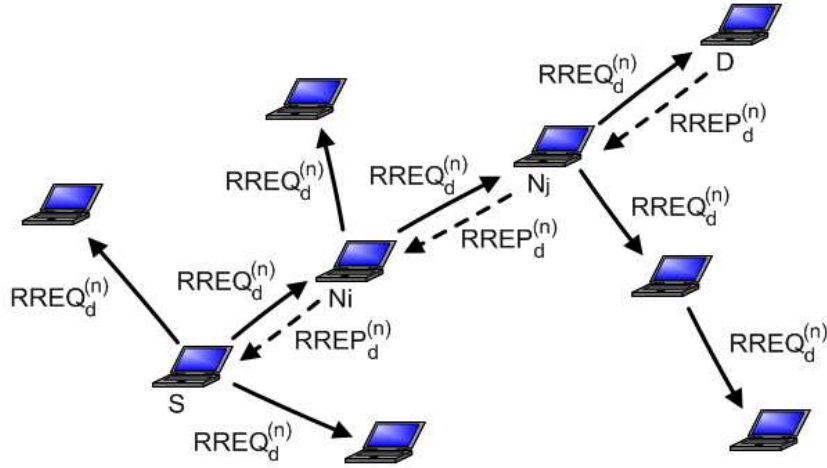


Figure 2.8: The Schematic Diagram of the Network Topology with the DSR Protocol

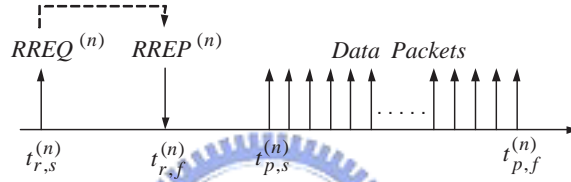


Figure 2.9: The Timing Diagram of the DSR Protocol

to construct the requested route to D . Until the destination node D is found in the route discovery process, a route reply ($RREP_d^{(n)}$) packet, which contains the complete route from S to D (i.e. $RREP_d^{(n)}\langle Adr_S, Adr_{N_i}, Adr_{N_j}, Adr_D \rangle$) as in Fig. 2.9, is sent back to the source node S at time $t_{r,f}^{(n)}$. The source node S will utilize the route to initiate data transmission to D between the time instants $t_{p,s}^{(n)}$ and $t_{p,f}^{(n)}$.

$t_{r,s}^{(n)}$: The starting time instant for sending the RREQ packet at the n^{th} route request

$t_{r,f}^{(n)}$: The time instant for receiving the RREP packet at the n^{th} route request

$t_{p,s}^{(n)}$: The starting time instant for packet delivery at the n^{th} route request

$t_{p,f}^{(n)}$: The ending time for packet delivery at the n^{th} route request

$t_{l,s}^{(n)}$: The starting time instant for sending the LREQ packet at the n^{th} route request

$t_{l,f}^{(n)}$: The time instant for receiving the LREP packet at the n^{th} route request

- $t_e^{(n)}$: The time instant for receiving the RERR packet at the n^{th} route request
- $t_m^{(n)}$: The time instant for receiving the proactive maintenance packet at the n^{th} route request
- $t_{r,s}^{(n+1)}$: The starting time instant for sending the RREQ packet at the $(n+1)^{th}$ route request
- $t_{r,f}^{(n+1)}$: The time instant for receiving the RREP packet at the $(n+1)^{th}$ route request
- $t_{p,s}^{(n+1)}$: The starting time instant for packet delivery at the $(n+1)^{th}$ route request
- $t_{p,f}^{(n+1)}$: The ending time for packet delivery at the $(n+1)^{th}$ route request

2.3.3 The Location-Aided Routing (LAR) Protocol

The Location Aided Routing (LAR) protocol is also an on-demand routing algorithm [22]. With the assistance of MN's position information, the algorithm restricts the packet flooding area in the route discovery process in stead of spreading out to the whole region as in the DSR algorithm.

Location services are required for the location-based routing algorithms to obtain the position information of the destination node before the route discovery process. As shown in Fig. 2.10, the location service request ($LREQ_l^{(n)}(Adr_S, Adr_D)$) initiated by S at time $t_{l,s}^{(n)}$ is transmitted to its neighboring MNs using the flooding mechanism. The location service reply ($LREP_l^{(n)}$) is received by S at time $t_{l,f}^{(n)}$ while the location information of D is available, i.e. $LREP_l^{(n)}(Adr_S, Adr_D, P_D(t_l^{(n)}), V_D(t_l^{(n)}))$. It is noted that $P_D(t_l^{(n)})$ and $V_D(t_l^{(n)})$ represent D 's latest position and velocity that are obtained by D at the time instant $t_l^{(n)}$, where $t_l^{(n)} = \{t \in \mathfrak{R} | 0 < t \leq t_{l,f}^{(n)}\}$ is determined by the frequency of D 's location updates.

One of the commonly used LAR algorithms, called the LAR-Box, defines a *Request Zone* ($RZ_l^{(n)}$) as shown in Fig. 2.10. It is a rectangular box determined by the source and the destination nodes. The circle, called *Expected Zone* in the LAR-Box algorithm, is centered at the destination position $P_D(t_l^{(n)})$. The radius of the *Expected Zone* ($R_l^{(n)}$) at the n^{th} route request is determined by S , which is defined as $R_l^{(n)} = V_D(t_l^{(n)}) \cdot \Delta t_l^{(n)}$ where $\Delta t_l^{(n)} = (t_{r,s}^{(n)} - t_l^{(n)})$. The limited region $RZ_l^{(n)}$ is determined by the positions of S and D and $R_l^{(n)}$, i.e. $RZ_l^{(n)} = \Gamma_l(P_S(t_{r,s}^{(n)}), P_D(t_l^{(n)}), R_l^{(n)})$. After obtaining the information from

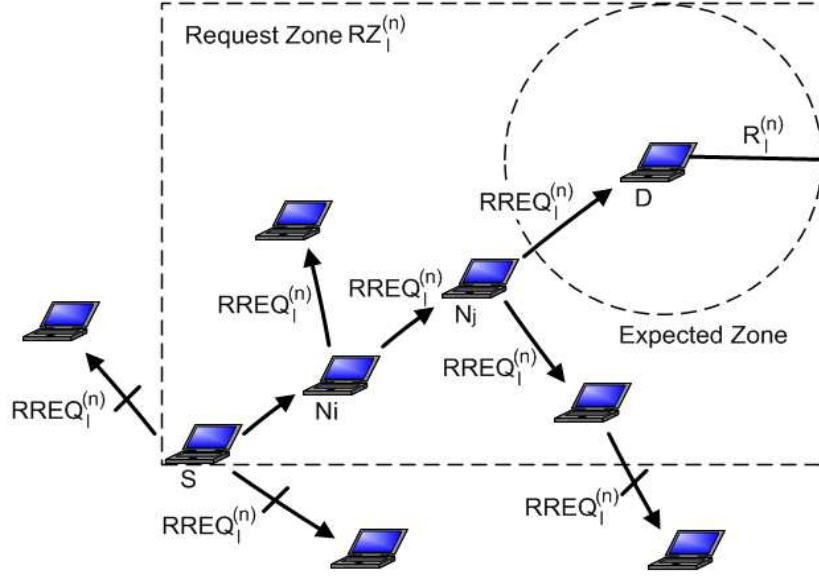


Figure 2.10: The Schematic Diagram of the Network Topology with the LAR Protocols

the location service, S initiates the route request at time $t_{r,s}^{(n)}$ as $RREQ_l^{(n)} \langle RREQ_d^{(n)}, RZ_l^{(n)} \rangle$. The additional information in the $RREQ_l^{(n)}$ is utilized for the intermediate MN to determine if itself is located within the confined region $RZ_l^{(n)}$. The route discovery process ended at time $t_{r,f}^{(n)}$ after the information of D is acquired by S with $RREP_l^{(n)} \langle RREP_d^{(n)}, P_D(t_r^{(n)}), V_D(t_r^{(n)}) \rangle$. The updated location information of D is acquired by S at time $t_r^{(n)} = \{t \in \mathfrak{R} | t_l^{(n)} < t \leq t_{r,f}^{(n)}\}$. The efficiency for route search can be increased with the constrained area of flooding. The source node S utilizes the route obtained from $RREP_l^{(n)}$ to transmit data packets to D between the time instants $t_{p,s}^{(n)}$ and $t_{p,f}^{(n)}$.

As shown in Fig. 2.11, a new route request $RREQ_l^{(n+1)}$ is started either another data transmission is initiated from S or a $RERR^{(n)}$ packet is received by S at time $t_e^{(n)}$ in the n^{th} route request. The route repairing mechanism for both the DSR and the LAR-Box algorithms is to initiate a route error ($RERR^{(n)}$) packet from the broken link back to S . The $RREQ_l^{(n+1)} \langle RREQ_d^{(n+1)}, RZ_l^{(n+1)} \rangle$ and $RREP_l^{(n+1)} \langle RREP_d^{(n+1)}, P_D(t_r^{(n+1)}), V_D(t_r^{(n+1)}) \rangle$ can be obtained with similar procedures, where

$$RZ_l^{(n+1)} = \Gamma_l(P_S(t_{r,s}^{(n+1)}), P_D(t_r^{(n)}), R_l^{(n+1)})$$

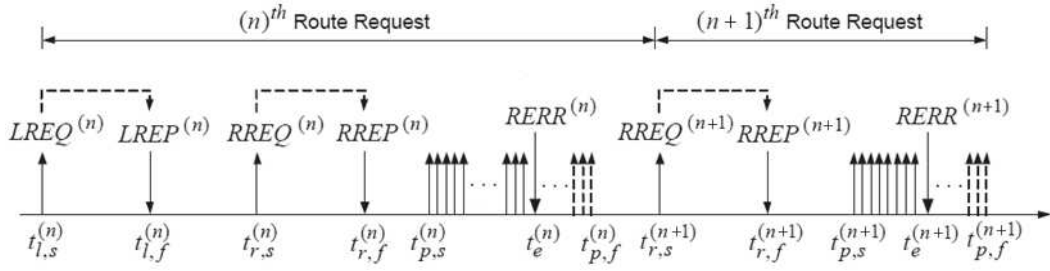


Figure 2.11: The Timing Diagram of the LAR Protocols

$$\begin{aligned}
 R_l^{(n+1)} &= V_D(t_r^{(n)}) \cdot (t_{r,s}^{(n+1)} - t_r^{(n)}) \\
 &= V_D(t_r^{(n)}) \cdot \Delta t^{(n)}
 \end{aligned}$$

with $t_r^{(n+1)} = \{t \in \mathfrak{R} | t_r^{(n)} < t \leq t_{r,f}^{(n+1)}\}$ as the time instant for the most recent location update before time $t_{r,f}^{(n+1)}$.



Chapter 3

Mobility Models

In this chapter, four mobility models, the Gauss-Markov Mobility (GMM) model, the Constant Speed Mobility (CSM) model, the Random Waypoint Mobility (RWM) model, and the Highway Mobility (HM) model, are presented. The GMM and CSM will be utilized as two separate cases to predicted the MN's movement in the design of the proposed VAR routing algorithm. Since different types of MN mobility affect the performance of the designed ad hoc routing algorithms, it is therefore important to construct feasible mobility models for simulation purpose that emulate the realistic moving environment. The RWM and HM will be described to generate the realistic motion of each MN.

3.1 The Gauss-Markov Mobility (GMM) Model

The Gauss-Markov Mobility Model [34] is adapted in this thesis to represent the motion of each MN. The moving direction α_k (*w.r.t.* the positive x -axis) and the speed V_k of each MN at a discrete time instant t_k can be formulated as [35]:

$$\alpha_k = \gamma_1 \alpha_{k-1} + (1 - \gamma_1) \bar{\alpha} + \sqrt{(1 - \gamma_1^2)} X_{\alpha_{k-1}} \quad (3.1)$$

$$V_k = \gamma_2 V_{k-1} + (1 - \gamma_2) \bar{V} + \sqrt{(1 - \gamma_2^2)} X_{V_{k-1}} \quad (3.2)$$

where $\bar{\alpha}$ and \bar{V} represent the asymptotic mean of the moving direction and the speed as $t_k \rightarrow \infty$; $X_{\alpha_{k-1}}$ and $X_{V_{k-1}}$ are zero mean Gaussian distributed random variables; γ_1 and γ_2 are tunable parameters that represent different levels of randomness as $0 \leq \gamma_i \leq 1$, for $i = 1, 2$. The two extreme cases correspond to linear motion (as $\gamma_i = 1$) and Brownian motion (as $\gamma_i = 0$). The benefit of using the GMM model for the MN's movement is that it preserves certain levels of (i) motion randomness and (ii) memories from previous time steps as the parameters γ_i varies. A more realistic motion trajectory can be obtained with the GMM model comparing with the Random Walk Mobility Model [36], which results in sharp turns and sudden stops. With (3.1) and (3.2), the position $P(x_k, y_k)$ of the MN at the time instant t_k becomes

$$x_k = x_{k-1} + V_{k-1} \delta t \cos \alpha_{k-1} \quad (3.3)$$

$$y_k = y_{k-1} + V_{k-1} \delta t \sin \alpha_{k-1} \quad (3.4)$$

where δt is the sampling interval between the time instant t_k and its previous time instant t_{k-1} . It is assumed that the position information of a MN, including its position $P(x_i, y_i)$, velocity V_i , and the heading angle α_i , is obtained at the time instant t_i via its positioning system. $P(x_j, y_j)$ is the predicted position of the MN at the time instant t_j as $t_j \geq t_i$. The traveling distance $(\Delta x_{i,j}, \Delta y_{i,j})$ of the MN within the time duration $\Delta t_{i,j} = (t_j - t_i)$ can be obtained by summing along the x and y directions from (3.3) and (3.4):

$$\Delta x_{i,j} = \sum_{k=i+1}^j V_k \delta t \cos \alpha_k \quad (3.5)$$

$$\Delta y_{i,j} = \sum_{k=i+1}^j V_k \delta t \sin \alpha_k \quad (3.6)$$

It is noted that α_k and V_k represent the moving direction and speed of the MN at the time instant t_k , which can be obtained from (3.1) and (3.2).

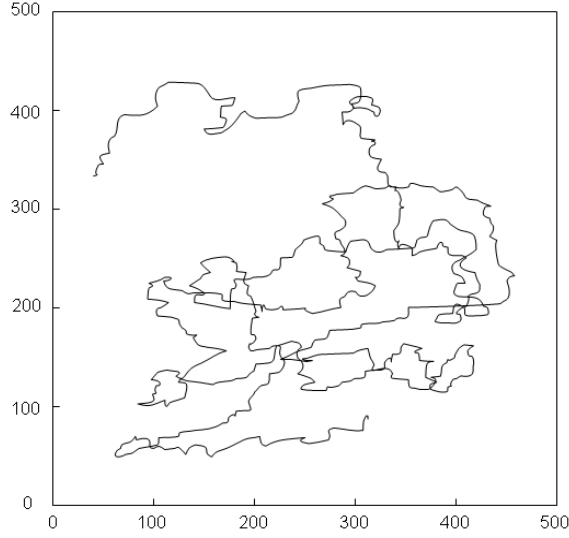


Figure 3.1: The motion of the MN using Gauss-Markov Mobility Model

3.1.1 Parameter Estimation of the Gauss-Markov Mobility Model

As discussed in the previous section, γ_{1D} and γ_{2D} represent the level of randomness for the corresponding moving angle (α_k) and speed (V_k) of the MN. In order to facilitate solving these two parameters, both (3.1) and (3.2) can be rewritten into the following format:

$$\alpha_k = \begin{bmatrix} \alpha_{k-1} & \bar{\alpha} \end{bmatrix} \begin{bmatrix} \gamma_1 \\ 1 - \gamma_1 \end{bmatrix} + \sqrt{(1 - \gamma_1^2)}X \quad (3.7)$$

$$v_k = \begin{bmatrix} v_{k-1} & \bar{V} \end{bmatrix} \begin{bmatrix} \gamma_2 \\ 1 - \gamma_2 \end{bmatrix} + \sqrt{(1 - \gamma_2^2)}X \quad (3.8)$$

and compared with linear model:

$$z_k = \underline{h}_k^T \underline{\gamma} + v_k \quad (3.9)$$

where \underline{h}_k is a 2×1 vector, v_k is the random noise term, and $\underline{\gamma}$ is the time-varying unknown value of the parameter vector of interest. It is noted that the v_k and α_k are updated every 1

sec in average.

Parameter Estimation Using Least Mean Square (LMS)

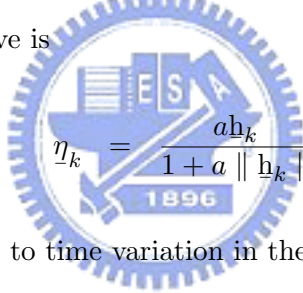
The parameter $\underline{\gamma}$ can be estimated recursively by:

$$\hat{\underline{\gamma}}_k = \mathbf{A}_{k-1} \hat{\underline{\gamma}}_{k-1} - \underline{\eta}_k (\underline{h}_k^T \mathbf{A}_{k-1} \hat{\underline{\gamma}}_{k-1} - z_k) \quad (3.10)$$

where \mathbf{A}_k is a potentially time-varying $p \times p$ matrix and $\underline{\eta}_k$ is some appropriately chosen $p \times 1$ gain vector. In LMS, \mathbf{A}_k is set to \mathbf{I}_p for all k . The normalized LMS algorithm has a gain vector of

$$\underline{\eta}_k = a \underline{h}_k \quad (3.11)$$

where $a > 0$ is a constant scale factor useful in tracking problems. An often-used normalized variation on the basic form above is

$$\underline{\eta}_k = \frac{a \underline{h}_k}{1 + a \|\underline{h}_k\|} \quad (3.12)$$


which sometimes helps to adapt to time variation in the system by scaling for different magnitudes in the design vector \underline{h}_{k+1} .

Parameter Estimation Using Recursive Least Square (RLS)

The parameter $\underline{\gamma}$ can also be obtained by RLS and the following procedure are needed:

$$\underline{\pi}_k = \mathbf{P}_{k-1} \underline{h}_k \quad (3.13)$$

$$\underline{\eta}_k = \frac{\underline{\pi}_k}{\lambda + \underline{h}_k^H \underline{\pi}_k} \quad (3.14)$$

$$\underline{\xi}_k = z_k - \underline{\gamma}_{k-1}^H \underline{h}_k \quad (3.15)$$

$$\underline{\gamma}_k = \underline{\gamma}_{k-1} + \underline{\eta}_k \underline{\xi}_k \quad (3.16)$$

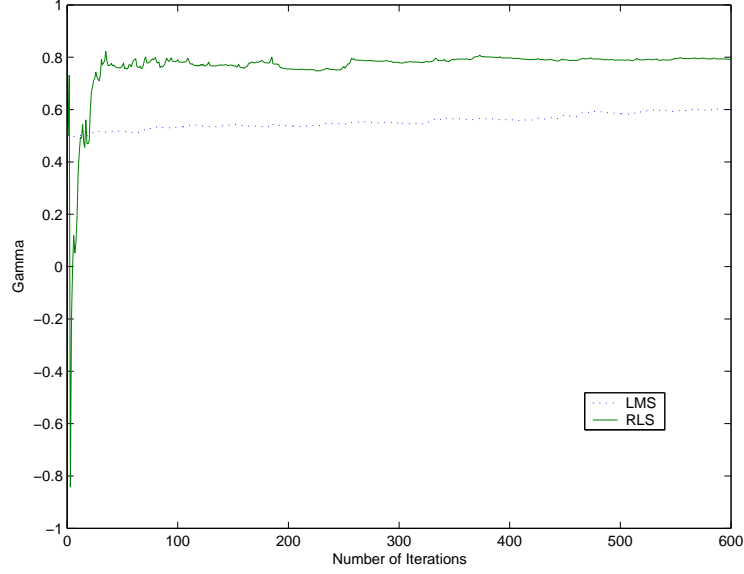


Figure 3.2: compare LMS and RLS

and

$$\mathbf{P}_k = \lambda^{-1} \mathbf{P}_{k-1} - \lambda^{-1} \eta_k \mathbf{l}_k^H \mathbf{P}_{k-1} \quad (3.17)$$

As shown in Fig. 3.2, v_k is estimated by LMS and RLS. The data is generated by GMM with underlying $\gamma = 0.8$ and $\bar{V} = 5m/s$. The tunable variables are set $a = 0.00008$ in LMS and $\lambda = 0.99999$ in RLS. It can be seen that the RLS algorithm converges faster than LMS, and needs about 50 samples (i.e. 50 seconds in average).

Due to the dynamic motion behavior of MN, the underlying γ is a time varying parameter. In Fig. 3.3, the RLS are compared with LMS under different tunable variable a and λ . It can be seen that RLS can adapt faster than LMS when the parameter γ changes from 0.8 to 0.2 at 1500th sample.

3.2 The Constant Speed Mobility (CSM) Model

In the previous subsection, the GMM model is utilized to obtain the predicted information (including the speed V_j and the moving direction α_j) of an MN based on its previous motion

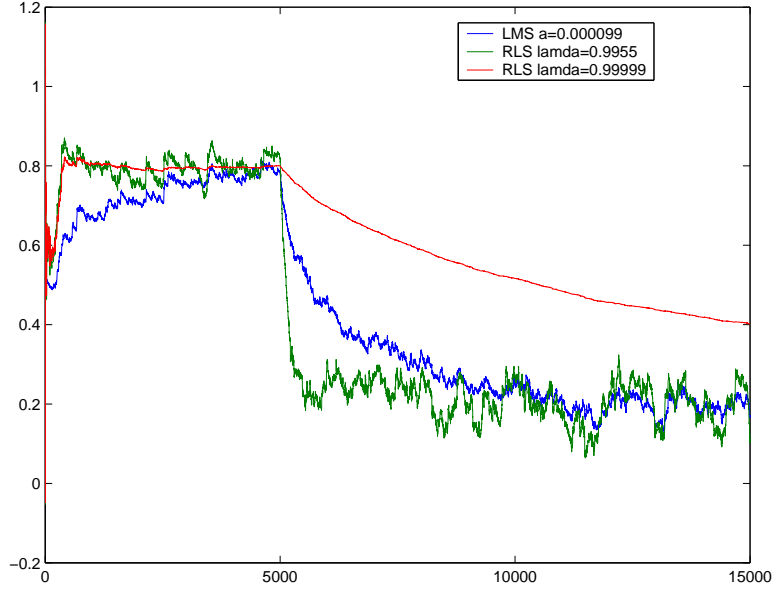


Figure 3.3: Estimation of time varying Parameter

states. In some cases, however, it is possible to assume that the MN remains constant speed (V_o) along the same moving direction (α_o) within the time interval $\Delta t_{i,j} = (t_j - t_i)$, i.e. $V(t) = V_o$ and $\alpha(t) = \alpha_o$ for $t \in [t_i, t_j]$. The traveling distance of the MN along the x and y directions ($\Delta x_{i,j}$, $\Delta y_{i,j}$) within the time duration $\Delta t_{i,j}$ can therefore be simplified from (3.5) and (3.6) as:

$$\Delta x_{i,j} = V_o \Delta t_{i,j} \cos \alpha_o \quad (3.18)$$

$$\Delta y_{i,j} = V_o \Delta t_{i,j} \sin \alpha_o \quad (3.19)$$

The constant speed assumption in the CSM model is applicable while the MN moves in a constant speed (along with the same direction) manner. This scenario is possible to happen in constrained topologies with similar traffic flows, including city streets and highway topologies. With the constant speed assumption, the CSM model provides less expensive computation cost comparing with the GMM model. The CSM model is treated as a special case for simple motion prediction. The routing performance of the VAR algorithm using the CSM model will be compared with that using the GMM model in the simulations.

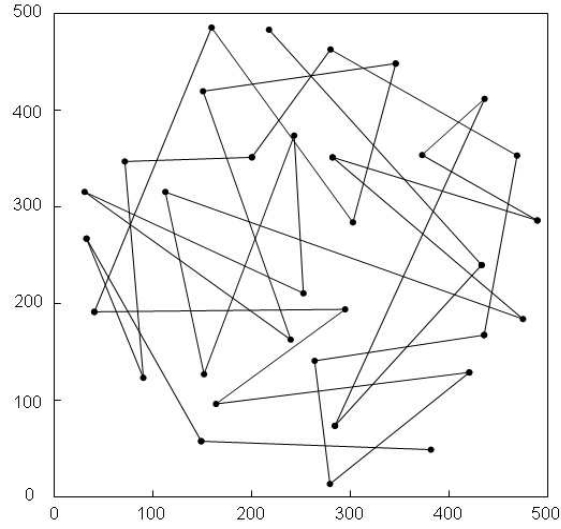


Figure 3.4: The motion of the MN using Random Waypoint Mobility Model

3.3 The Random Waypoint Mobility (RWM) Model

The Random Waypoint Mobility Model (RWMM) is widely used to evaluate the performance of ad hoc routing protocols [15] [16] [36]. There are two important parameters, v_{max} and t_{pause} , used to describe the moving behavior in Random Waypoint Mobility Model. As the simulation starts, the mobile node randomly chooses a position as its destination with the uniformly distributed speed form $[0, v_{max}]$. when node reaches the destination, it stops for time duration t_{pause} . After t_{pause} time expired, the node chooses another destination with a new speed and moves towards it. The process is repeating until the simulation ends. As shown in Fig. 3.4, the straight line corresponds to the MN's trajectory from one pausing point to another.

3.4 The Highway Mobility (HM) Model

In this thesis, a Highway Mobility (HM) model is developed to evaluate the effectiveness of the proposed algorithms via simulations. As shown in Fig. 3.5, the following scenarios are considered in the proposed HM model to closely emulate real traffic environments (such as highways and city streets):

1. A bi-directional four-lane street (two lanes in each direction) is assumed in the HM model.
2. In the moving direction (i.e. MNs move along the x direction at the lower two lanes and along the $-x$ direction at the upper two lanes), the MNs should maintain their speeds based on an average speed, which is pre-specified for each lane.
3. The MNs may deviate within the lane for certain degree in the lateral direction (i.e. along the y direction).
4. Lane changes are allowed in the HM model. If the speed of the MN at slow (fast) lane is larger (smaller) than a pre-defined value, the MN should start the lane-changing process.

The HM model that satisfies the above traffic scenarios can be formulated by modifying the GMM model as described in Chapter 3.1. In the HM model, the motion equation of MNs along the x direction is represented by x_k as in (3.3). The associated V_k is obtained from (3.2), where \bar{V} is selected based on the average speed of each lane. The moving direction α_k should be confined to the lane direction with small variations due to different driving behaviors. α_k can be modified from (3.1) by setting $\gamma = 0$ as:

$$\alpha_k = \bar{\alpha} + X_{\alpha_{k-1}} \quad (3.20)$$

where $\bar{\alpha} = 0$ (or π) for moving along the positive (or negative) x direction. The zero-mean Gaussian distributed random variable $X_{\alpha_{k-1}}$ is varied based on a pre-assumed driving deviation. The lateral displacement y_k can be modified from (3.4) as:

$$y_k = y_0 + V_{k-1} \delta t \sin \alpha_{k-1} \quad (3.21)$$

where y_0 is a constant value (i.e. $y_0 = y_{slow}$ for slow lane and $y_0 = y_{fast}$ for fast lane) depending on the initial position of the MN along the y direction. The reason of using a constant y_0 is to simulate the driving behavior of maintaining the MN on the center of a lane.

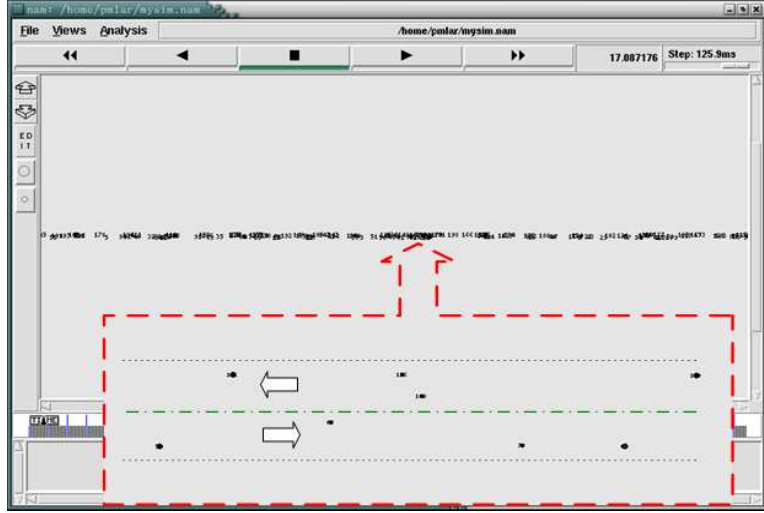


Figure 3.5: The motion of the MN using Constant Speed Mobility Model

Fig. 3.6 shows the state diagram for the lane-changing scenarios. The Probability Distribution Function (PDF) of the MN's speed V_k is denoted as $f_{V_k}(v)$, where V_k is a Gaussian distributed random variable (as can be observed from Eqn. (3.2)). In order to satisfy the conditions for lane change, the following Cumulative Distribution Functions (CDFs) are defined:

- $F_1 = \sum_{v: v > V_{upper}} f_{V_k}(v)$: F_1 is the CDF when the MN's speed V_k is greater than the upper speed threshold V_{upper} . As shown in Fig. 3.6, the MN will move to the fast lane if it is currently in the slow lane.
- $F_2 = \sum_{v: v < V_{lower}} f_{V_k}(v)$: F_2 is the CDF when the MN's speed V_k is smaller than the lower speed threshold V_{lower} . The MN will move to the slow lane if it is currently in the fast lane.
- $F_3 = \sum_{v: V_{lower} \leq v \leq V_{upper}} f_{V_k}(v)$: F_3 is the CDF when the MN's speed V_k lies between the lower and upper speed limits. The MN will remain in its current state.

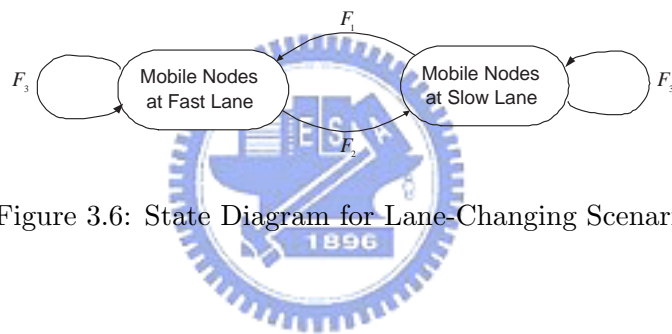


Figure 3.6: State Diagram for Lane-Changing Scenario

Chapter 4

The Proposed Mobility and Location-Based Routing Protocols

As indicated in the survey on position-based routing algorithms [27], the location services and the packet forwarding strategies are the two major components in the protocol design. The primary purpose of the location services are to provide the position information of the destination node for the source node. Based on the information, the position-aware routing protocols can determine their packet forwarding strategies. Most of the position-aware routing protocols utilize global flooding [21]- [23] as the location services, which result in significant degradation in routing efficiency. The GLS alleviates the problem by providing location updates within the local area of the network. A small set of MNs are served as location servers to offer location information for their neighborhoods. The appropriate selection of the location servers influences the performance of the location updates within the GLS scheme. A comparative studies between location-based ad hoc routing protocols can be obtained as in [28] [29].

On the other hand, different types of the MN's mobility models have been studied in many research [30]- [32]. It has been observed that the mobile models utilized in the ad hoc network simulation greatly influence the routing performance. The commonly used random waypoint mobility model (as was utilized in [15] [16]) is found to be insufficient in most of

the realistic scenarios [33]. Different types of mobility models have been proposed to emulate the motion behaviors of the MNs. It is suggested that the designed ad hoc routing protocols should be evaluated under the various types of the MN's mobility models in order to satisfy the requirements for realistic situations.

However, the mobility patterns of the MNs have not been taken into consideration in most of the location-based routing protocol design. Since the velocity and heading angle of the MN are obtainable from the positioning systems, it is practicable to incorporate the information in the design of ad hoc routing protocols. The proposed Velocity Aided Routing (VAR) algorithm determines its packet forwarding scheme by calculating the relative velocity between the potential forwarding nodes and the destination node. This scheme forwards the data packets via those intermediate nodes that are faster approaching the destination node. The Gauss-Markov Mobility (GMM) Model [34] [35] and the Constant Speed Mobility (CSM) Model are utilized in the design of the VAR algorithm to compute the MN's speed and moving angle. The benefit of using the GMM model is that it can be utilized to adaptively emulate possible moving behavior with certain levels of linear and Brownian motions. It is shown in the paper that the proposed VAR algorithm are especially feasible for topologies with confined shapes and dynamic characteristics (e.g. highways, city streets). It will also be shown in the simulation results that the GMM-based VAR algorithm provides better routing performance comparing with the CSM-based VAR algorithm.

Moreover, since mobility of the MNs diverse under different moving scenarios, it will be beneficial to incorporated the MN's predicted movement in the design of routing protocols. The proposed Predictive Mobility and Location-Aware Routing (PMLAR) algorithm determines its packet forwarding scheme by predicting the current and the future position of the destination node. The prediction mechanism defines the packet forwarding region by adapting its adjustable parameters based on the previous moving behavior of the destination node. The GMM model is also utilized in the design of the PMLAR algorithm. It is shown in this paper that the proposed PMLAR algorithm is feasible for different types of network topologies. The PMLAR-V algorithm further incorporate the VAR algorithm to effectively improve

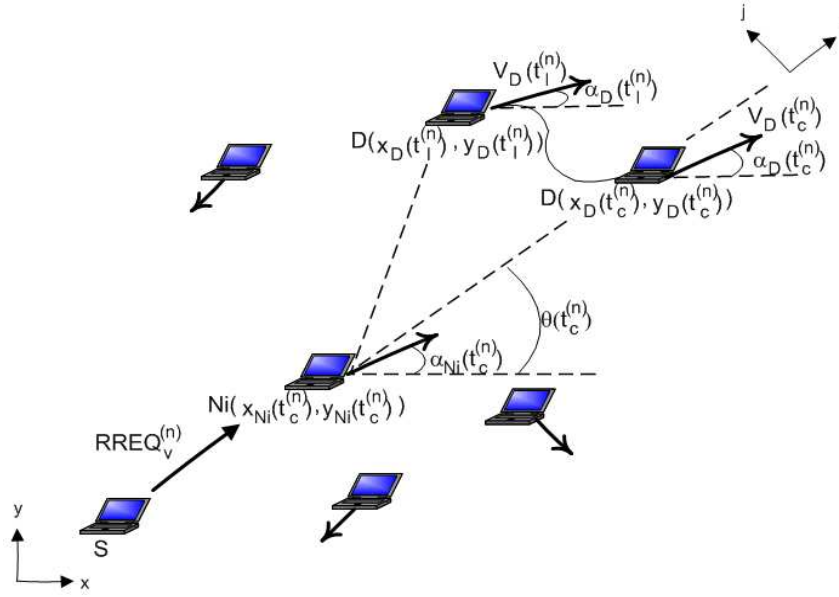


Figure 4.1: Schematic Diagram of the VAR Schemes using the Gauss-Markov Mobility Model

the end-to-end delay performance. In additions, the PMLAR-PV enhance the pakcet delivery ratio by adopting a mechanism for proactive maintenance.

Two mobility models, the Highway Mobility (HM) model and the Random Waypoint Mobility (RWM) model, are implemented in simulations to offer different types of simulation scenarios. The effectiveness of the VAR, PMLAR, PMLAR-V, and PMLAR-PV algorithms is evaluated and compared with other existing routing protocols via simulations.

4.1 The Velocity Aided Routing (VAR) Protocol

In this section, the proposed Velocity Aided Routing (VAR) algorithm is presented. The proposed algorithm determines the feasible MNs for packet forwarding based on the relative velocity between the forwarding node N_i and the destination node D . The VAR algorithm is designed by predicting the motion of D using either the GMM model or the CSM model as shown in the next two subsections:

4.1.1 The VAR using the Gauss-Markov Mobility Model (VAR-GMM)

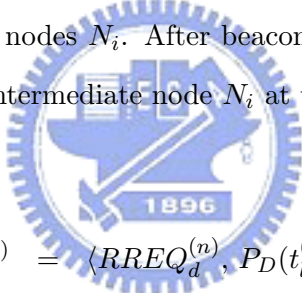
Fig. 4.1 shows the schematic diagram of the VAR algorithm using the GMM model. The timing model as shown in Fig. 2.11 is also feasible for the VAR algorithm. Comparing with the LAR-Box protocol, the location service for the VAR algorithm should provide additional information of D in its location service reply packet as:

$$LREQ_v^{(n)} = \langle LREQ_l^{(n)} \rangle \quad (4.1)$$

$$LREP_v^{(n)} = \langle LREP_l^{(n)}, \alpha_D(t_l^{(n)}), \gamma_{iD}(t_l^{(n)}) \rangle \quad (4.2)$$

where $\alpha_D(t_l^{(n)})$ is the moving angle of D obtained at time $t_l^{(n)}$ from its latest position update. The two tunable parameters of D , $\gamma_{iD}(t_l^{(n)})$ for $i = 1, 2$, are computed and acquired at the time instant $t_l^{(n)}$ by RLS.

After the location service process, S initiates a route discovery to the destination node D via some of the intermediate nodes N_i . After beaconing within the neighborhood of S , a $RREQ_v^{(n)}$ packet is sent to an intermediate node N_i at the time instant $t_{r,s}^{(n)}$ as:



$$RREQ_v^{(n)} = \langle RREQ_d^{(n)}, P_D(t_l^{(n)}), V_D(t_l^{(n)}), \alpha_D(t_l^{(n)}), \gamma_{iD}(t_l^{(n)}) \rangle \quad (4.3)$$

The location information of N_i , including its position $P_{N_i}(t_c^{(n)})$, velocity $V_{N_i}(t_c^{(n)})$, and heading angle $\alpha_{N_i}(t_c^{(n)})$, is obtained from its positioning system at the current time instant $t_c^{(n)}$. On the other hand, the location information of D (i.e. $P_D(t_l^{(n)})$, $V_D(t_l^{(n)})$, $\alpha_D(t_l^{(n)})$, and $\gamma_{iD}(t_l^{(n)})$) was obtained by S at a previous time instant $t_l^{(n)}$ and was forwarded to N_i via the $RREQ_v^{(n)}$ packet. By adopting the GMM model, the current location information of D (i.e. $P_D(t_c^{(n)})$, $V_D(t_c^{(n)})$, and $\alpha_D(t_c^{(n)})$) can be calculated from the previous time instant $t_l^{(n)}$ using (3.1) to (3.4).

The proposed VAR algorithm utilizes the following criterions to determine if the interme-

diate node N_i is suitable as the *forwarding node* for packet delivery:

$$\Delta V_i > [V_{N_i}(t_c^{(n)}) + V_D(t_c^{(n)})] \delta_{1,i} + \delta_{2,i} \quad (4.4)$$

$$|\Delta V_j| < [V_{N_i}(t_c^{(n)}) + V_D(t_c^{(n)})] \delta_{1,j} + \delta_{2,j} \quad (4.5)$$

where

$$\begin{aligned} \Delta V_i &= V_{N_i}(t_c^{(n)}) \cos(\theta(t_c^{(n)}) - \alpha_{N_i}(t_c^{(n)})) \\ &\quad - V_D(t_c^{(n)}) \cos(\theta(t_c^{(n)}) - \alpha_D(t_c^{(n)})) \end{aligned} \quad (4.6)$$

$$\begin{aligned} \Delta V_j &= V_{N_i}(t_c^{(n)}) \sin(\theta(t_c^{(n)}) - \alpha_{N_i}(t_c^{(n)})) \\ &\quad - V_D(t_c^{(n)}) \sin(\theta(t_c^{(n)}) - \alpha_D(t_c^{(n)})) \end{aligned} \quad (4.7)$$

As shown in Fig. 4.1, $\theta(t_c^{(n)})$ represents the angle between D and N_i at $t_c^{(n)}$, which can be calculated using (3.5) and (3.6) as:

$$\theta(t_c^{(n)}) = \tan^{-1} \frac{(y_D(t_l^{(n)})) - y_{N_i}(t_c^{(n)}) + (\Delta y_{l,c})_D}{(x_D(t_l^{(n)})) - x_{N_i}(t_c^{(n)}) + (\Delta x_{l,c})_D} \quad (4.8)$$

where the location information $(x_D(t_l^{(n)}), y_D(t_l^{(n)}))$ of D is obtained from the positioning system at the previous time instant $t_l^{(n)}$, and the location $(x_{N_i}(t_c^{(n)}), y_{N_i}(t_c^{(n)}))$ of N_i is acquired at the current time $t_c^{(n)}$.

It is noted that $\delta_{1,i}, \delta_{2,i} \geq 0$ and $\delta_{1,j}, \delta_{2,j} > 0$ in (4.4) and (4.5) are the tuning parameters for the VAR criterion. $\delta_{1,i}$ and $\delta_{1,j}$ represent speed dependent tuning coefficients. The first criterion (i.e. (4.4)) of the VAR algorithm indicates that the potential *forwarding node* N_i should move toward the destination node D along their connecting line (i.e. the i^{th} direction as shown in Fig. 4.1); while the second criterion (i.e. (4.5)) is used to limit the relative speed between N_i and D along their perpendicular direction j . With the VAR criterions, the amount of potential forwarding nodes within the constrained flooding area will be decreased.

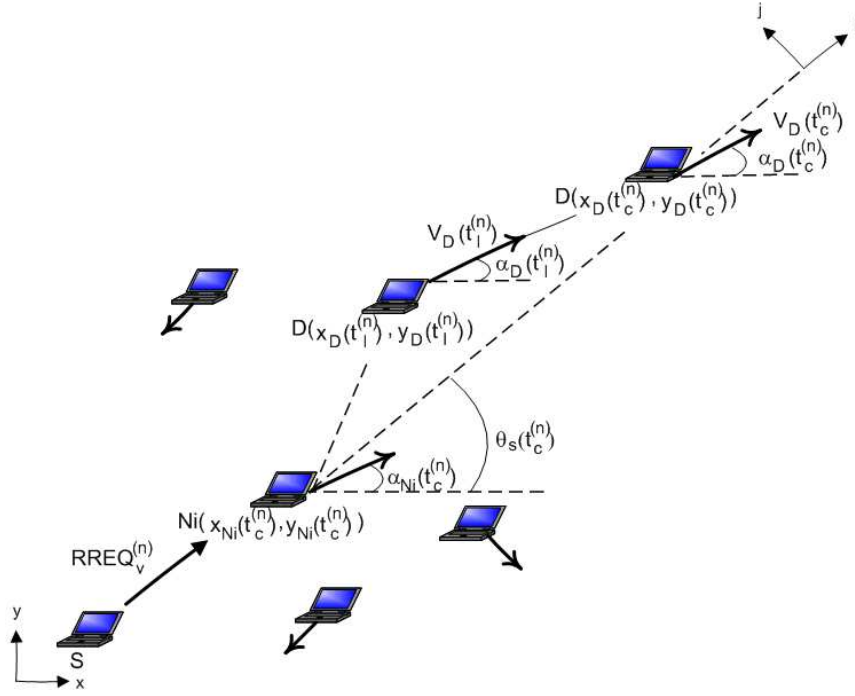


Figure 4.2: Schematic Diagram of the VAR Schemes using the Constant Speed Mobility Model

4.1.2 The VAR using the Constant Speed Mobility Model (VAR-CSM)

As described in the Chapter 3.2, it is feasible to assume the MN to pertain constant speed during the time interval $(t \in [t_l^{(n)}, t_c^{(n)}])$ in consideration. The VAR criterions (i.e. (4.4) - (4.7)) proposed as in the previous subsection are still applicable to be adopted in the CSM model. The only difference is that a simplified version of $\theta(t_c^{(n)})$ is obtained as shown in Fig. 4.2:

$$\theta_s(t_c^{(n)}) = \tan^{-1} \frac{(y_D(t_l^{(n)})) - y_{Ni}(t_c^{(n)}) + V_D(t_l^{(n)})\Delta t_{l,c} \sin \alpha_D(t_l^{(n)})}{(x_D(t_l^{(n)})) - x_{Ni}(t_c^{(n)}) + V_D(t_l^{(n)})\Delta t_{l,c} \cos \alpha_D(t_l^{(n)})} \quad (4.9)$$

where $\Delta t_{l,c} = (t_c - t_l)$. It can be seen that the computation complexity of $\theta_s(t_c^{(n)})$ is much less than the $\theta(t_c^{(n)})$ obtained from (4.8).

In both the VAR-GMM and the VAR-CSM algorithms, the $RREQ_v^{(n)}$ packet is flooded to all regions for route discovery, seeking for intermediate nodes that satisfy the criterions as in (4.4) and (4.5). After the route to D is constructed, a $RREP_v^{(n)}$ is returned to S at time $t_{r,f}^{(n)}$ as:

$$RREP_v^{(n)} = \langle RREP_l^{(n)}, \alpha_D(t_r^{(n)}), \gamma_{iD}(t_r^{(n)}) \rangle \quad (4.10)$$

The data packet will be transmitted between the time instants $t_{p,s}^{(n)}$ and $t_{p,f}^{(n)}$. Similar to the discussion as in the LAR protocol, a new route request will be initiated by S at time $t_{r,s}^{(n+1)}$. A new set of route request/reply will be adopted as:

$$RREQ_v^{(n+1)} = \langle RREQ_d^{(n+1)}, P_D(t_r^{(n)}), V_D(t_r^{(n)}), \alpha_D(t_r^{(n)}), \gamma_{iD}(t_r^{(n)}) \rangle \quad (4.11)$$

$$RREP_v^{(n+1)} = \langle RREP_l^{(n+1)}, \alpha_D(t_r^{(n+1)}), \gamma_{iD}(t_r^{(n+1)}) \rangle \quad (4.12)$$

4.2 The Predictive Mobility and Location-Aware Routing (PMLAR) Protocol

The proposed Predictive Mobility and Location-Aware Routing (PMLAR) Protocol will be explained in this section. The first subsection describes the prediction mechanism of the PMLAR protocol in details. The second subsection presents the PMLAR with the assistance of the Velocity Aided Routing (VAR) algorithm to increase the routing efficiency.

4.2.1 The PMLAR Protocol

The proposed PMLAR protocol is designed for S to predict the current and future location of D to achieve efficient data transmission. An enhanced location service is also considered in the proposed algorithm to address the potential indirect route between S and D . The three phases of the PMLAR algorithm (i.e. the location service, route discovery and packet forwarding, and route repairing) are stated as follow:

Location Service

The source node S intends to transmit data packets to the destination node D . However, S has no information about the position information of D at the beginning. It is required for S to activate a location service to obtain the position information of D . S will initiate a flooding process to send out the request packet to obtain D 's position information at time $t_{l,s}^{(n)}$ as shown in Fig. 2.11:

$$LREQ_p^{(n)} = \langle LREQ_v^{(n)} \rangle \quad (4.13)$$

After rebroadcasting by the intermediate node N_i , D is informed that a position request has been initiated by S . The up-to-date information of D , including the time stamp $t_l^{(n)}$, the position $P_D(t_l^{(n)})$, the velocity $V_D(t_l^{(n)})$, the moving angle $\alpha_D(t_l^{(n)})$, and the parameters $\gamma_{iD}(t_l^{(n)})$ are sent back to S via the reverse route. In addition, the position information of the forwarding nodes N_i , i.e. $\mathbf{P}_{N_i}^{(n)}(t_l^{(n)}) \equiv [P_{N_1}^{(n)}(t_l^{(n)}) \dots P_{N_n}^{(n)}(t_l^{(n)})]$, are also transmitted back to S via the $LREP_p^{(n)}$ packet as:

$$LREP_p^{(n)} = \langle LREP_v^{(n)}, \mathbf{P}_{N_i}^{(n)}(t_l^{(n)}) \rangle \quad (4.14)$$

The positions of the intermediate nodes $\mathbf{P}_{N_i}^{(n)}(t_l^{(n)})$ will be utilized in the route discovery phase to determine if an indirect region for packet forwarding is required.

Route Discovery and Packet Forwarding

S can start the processes of route discovery and forwarding of data packets after executing the location service. The prediction mechanism utilized in the proposed PMLAR algorithm is for S to predict the trajectory of D from its previous location update. As shown in Fig. 4.3, the trajectory \mathbf{P}' indicates the predictive path of D starting from the time instant $t_l^{(n)}$. It is noted that $t_l^{(n)}$ corresponds to the time instant that the location information of D is acquired

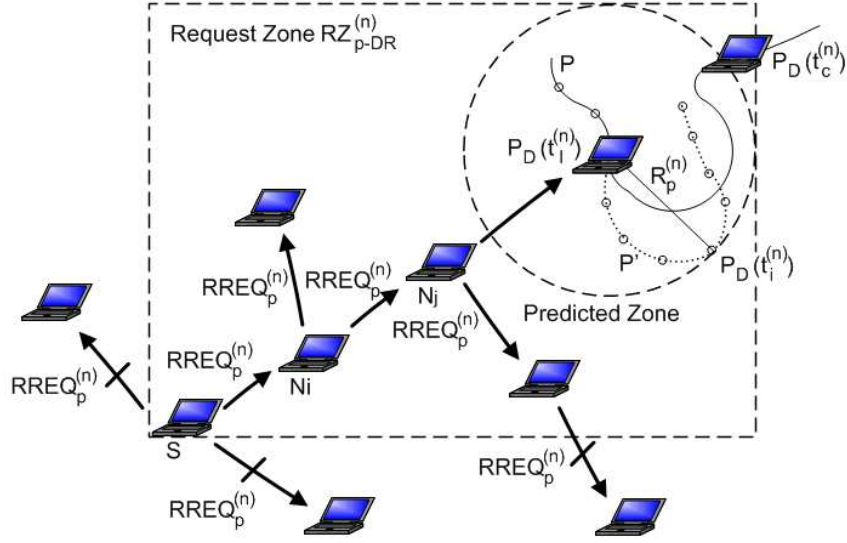


Figure 4.3: The Schematic Diagram of the Network Topology with the PMLAR Protocol

form positioning system. The current and future positions of D can be obtained at different predictive time steps as $\Delta T_l^{(n)} = \kappa \Delta t_l^{(n)} = \kappa(t_{r,s}^{(n)} - t_l^{(n)})$. As $\kappa = 1$, the current position of D is obtained; while the future position of D is predicted if $\kappa > 1$.

The prediction mechanism defines a *Predicted Zone* based on the trajectory of D . The *Predicted Zone* is defined as a circular region centered at $P_D(t_l^{(n)})$ with its radius $R_p^{(n)}$ defined as:

$$R_p^{(n)} = \max_{0 < i \leq \zeta} \left\{ [(\Delta x_{l,i})_D]^2 + [(\Delta y_{l,i})_D]^2 \right\}^{\frac{1}{2}} \quad (4.15)$$

where $(\Delta x_{l,i})_D$ and $(\Delta y_{l,i})_D$ can be obtained from (3.5) and (3.6); $\zeta = \Delta T_l^{(n)} / \delta t$ represents the total number of predicting steps. The distances from $P_D(t_l^{(n)})$ to the position of the i^{th} predicting step $P_D(t_i^{(n)})$ are calculated and the maximum value is selected as the radius of *Predicted Zone*. As shown in Fig. 4.3, the predicting mechanism starts at the time instant $t_l^{(n)}$ and the predicting trajectory by using the GMM model is shown in dotted line with empty circles. The predicting steps ζ equals to 8 in this case. The radius $R_p^{(n)}$ represents the predicted radius which happens at the 4th steps as in Fig. 4.3. Similar to the *Expected Zone* as in the LAR-Box algorithm, the *Predicted Zone* defines a circle that predict the potential

movement of the destination node D . However, the determination of the *Predicted Zone* is based on the predictive moving behavior of D , while the LAR-Box algorithm assumes constant moving speed of D along the time interval in consideration.

As the Predicted Zone is computed by S , either the Direct Routing (DR) or the Indirect Routing (IR) type will be determined. The parameter μ is utilized to exam the type of routing to be adopted:

$$\mu = \frac{\sum_{k=1}^n \|P_{N_{k+1}}^{(n)}(t_l^{(n)}) - P_{N_k}^{(n)}(t_l^{(n)})\|}{\|P_D^{(n)}(t_l^{(n)}) - P_S^{(n)}(t_{r,s}^{(n)})\|} \quad (4.16)$$

It is noted the position information as in (4.16) are acquired from $LREP_p^{(n)}$ as in (4.14). If $\mu \leq \pi$, the DR type of routing is utilized based on the geometric relationship as in Fig. 4.4. Similar to the LAR-Box algorithm, a rectangular box which encloses S 's position and the circle of radius $R_p^{(n)}$ is acquired (as shown in Fig. 4.3). The Request Zone ($RZ_{p-DR}^{(n)}$) can be obtained as:

$$RZ_{p-DR}^{(n)} = \Gamma_{DR}(P_S(t_{r,s}^{(n)}), P_D(t_l^{(n)}), R_p^{(n)}) \quad (4.17)$$

If $\mu > \pi$, the IR type of routing will be adopted. The criterion indicates that the accumulated distances between the intermediate MNs are comparably larger than half of the perimeter formed by the diameter as distance between S and D . A different type of Request Zone for the IR type of routing is illustrated as in Fig. 4.4. The positions of the intermediate node (i.e. $\mathbf{P}_{N_i}^{(n)}(t_l^{(n)})$) are utilized as the waypoints for the confined region. The Request Zone ($RZ_{p-IR}^{(n)}$) is obtained as:

$$RZ_{p-IR}^{(n)} = \Gamma_{IR}(P_S(t_{r,s}^{(n)}), P_D(t_l^{(n)}), R_p^{(n)}, \mathbf{P}_{N_i}^{(n)}(t_l^{(n)})) \quad (4.18)$$

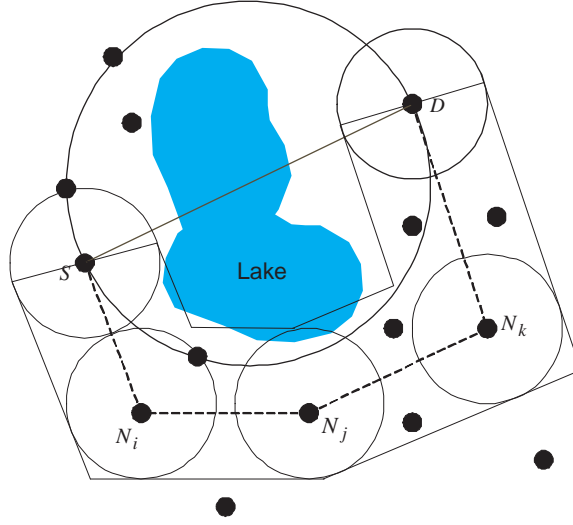


Figure 4.4: Schematic Diagram of the PMLAR Algorithm with Indirect Routing Scheme

A new route request ($RREQ_p^{(n)}$) packet will be sent out by S at time $t_{r,s}^{(n)}$ to initiate the route discovery process:

$$\begin{aligned}
 RREQ_p^{(n)} &= \langle RREQ_d^{(n)}, RZ_{p-IR}^{(n)} \rangle \quad \text{for } \mu > \pi \\
 &\langle RREQ_d^{(n)}, RZ_{p-DR}^{(n)} \rangle \quad \text{for } \mu \leq \pi
 \end{aligned} \tag{4.19}$$

The type of *Request Zone* selected in the $RREQ_p^{(n)}$ packet will depend on the magnitude of the parameter μ . After the route to D is established with the appropriate selection of the forwarding MNs, a $RREP_p^{(n)}$ is returned to S at time $t_{r,f}^{(n)}$ as:

$$RREP_p^{(n)} = \langle RREP_v^{(n)} \rangle \tag{4.20}$$

Thereafter, the data packet can be transmitted between the time instants $t_{p,s}^{(n)}$ and $t_{p,f}^{(n)}$.

Route Repairing

Due to the dynamic changes of network topologies, route maintenance and repairing should take place during data transmission from S to D . The PMLAR algorithm provides a repairing mechanism for broken transmission links.

Similar to the route error repair capability as in the DSR protocol [6], the source node S receives a route error ($RERR^{(n)}$) packet from one of the forwarding MNs if there exists a broken transmission link in the originally defined route. Assuming that the link is broken at the time instant $t_e^{(n)}$ ($t_{p,s}^{(n)} < t_e^{(n)} < t_{p,f}^{(n)}$) as in Fig. 2.11, the source node S will start a new route discovery process (i.e. the $(n+1)^{th}$ route request). A new *Request Zone* is utilized as the confined region for the selection of the packet forwarding nodes. A new set of route request/reply will be adopted as:

$$RREQ_p^{(n+1)} = \begin{cases} \langle RREQ_d^{(n+1)}, RZ_{p-IR}^{(n+1)} \rangle & \text{for } \mu > \pi \\ \langle RREQ_d^{(n+1)}, RZ_{p-DR}^{(n+1)} \rangle & \text{for } \mu \leq \pi \end{cases} \quad (4.21)$$

$$RREP_p^{(n+1)} = \langle RREP_v^{(n+1)} \rangle \quad (4.22)$$

4.2.2 The PMLAR Protocol with VAR Algorithm (PMLAR-V)

The prediction mechanism as described in the PMLAR protocol defines the *Predicted Zone* which predicts the potential future position of the destination node D . All of the intermediate nodes within the *Request Zone* (as shown in Fig. 4.3) are considered as potential forwarding nodes for packet forwarding. However, it is possible to further impose additional constraints on the selection of the intermediate nodes. Since the velocity information of the MNs are available from most of the positioning systems, it is reasonable to incorporate MN's velocity information as an additional criterion to determine if the MN is the feasible node for packet forwarding from S to D .

By combining (4.3) and (4.19), a new route request ($RREQ_{p-v}^{(n)}$) packet will be sent out

by S at time $t_{r,s}^{(n)}$ to initiate the route discovery process:

$$\begin{aligned}
RREQ_{p-v}^{(n)} = & \langle RREQ_d^{(n)}, RZ_{p-IR}^{(n)}, P_D(t_l^{(n)}), V_D(t_l^{(n)}), \\
& \alpha_D(t_l^{(n)}), \gamma_{iD}(t_l^{(n)}) \rangle \quad \text{for } \mu > \pi \\
& \langle RREQ_d^{(n)}, RZ_{p-DR}^{(n)}, P_D(t_l^{(n)}), V_D(t_l^{(n)}), \\
& \alpha_D(t_l^{(n)}), \gamma_{iD}(t_l^{(n)}) \rangle \quad \text{for } \mu \leq \pi
\end{aligned} \tag{4.23}$$

After receiving the $RREQ_{p-v}^{(n)}$ packet from S , N_i will perform the VAR algorithm (based on the criteria as in (4.4) and (4.5)) to determine if itself is a suitable node for packet forwarding. If the VAR criteria are satisfied, N_i will record itself on the routing information within the $RREQ_{p-v}^{(n)}$ packet header and rebroadcast the packet to N_j . The destination node D is informed that a request for data transmission is initiated by S after receiving the $RREQ_{p-v}^{(n)}$ packet. D will send out the route reply ($RREP_{p-v}^{(n)}$) packet to S via the reverse route which is recorded on the $RREQ_{p-v}^{(n)}$ packet header. The $RREP_{p-v}^{(n)}$ is returned to S at time $t_{r,f}^{(n)}$ as:

$$RREP_{p-v}^{(n)} = \langle RREP_v^{(n)} \rangle \tag{4.24}$$

After completing the route discovery process, the data packets can be delivered from S to D via the designated route.

It is noted that in the original VAR algorithm, the $RREQ_v^{(n)}$ packet is flooded to all regions for route discovery, seeking for intermediate nodes that satisfy the criteria as in (4.4) and (4.5). With the constraint of limiting the searching area within the *Request Zone*, the inefficiency occurred by the all-region flooding can be reduced. The selections of the potential forwarding nodes can therefore be confined within the predefined region. In the next section, simulations will be performed to evaluate the effectiveness of the VAR algorithms within the PMLAR protocol.

Chapter 5

Performance Evaluation

In this chapter, the parameter estimation and simulation results of proposed VAR and PMLAR are presented. The question arises in determination of the randomness of RWM and HM model. In order to estimate the underlying γ using RLS algorithm as mention in Chapter 3.1.1, the GMM model are borrowed from Chapter 3.1 to represent RWM and HM model in the form of GMM model. All the related variables of RLS algorithm will be decided in Chapter 5.1. The following three metrics are considered for performance comparison: data packet delivery ratio, end-to-end delay, and control packet overhead. With these metrics the VAR are evaluated using different predicting models and PMLAR are compared with the variety of existing protocols in Chapter 5.2.

5.1 Parameter Estimation

In this section, the RWM and HM model are modeled by GMM model. The different scenarios are also provided to obtain the value of λ which determines the convergence rate and the variance of γ_1 and γ_2 .

5.1.1 Parameter Estimation of RWM Model

The heading angle of RWM model will move toward certain direction (i.e. $\bar{\alpha}$) during linear motion and change direction after random motion. The α_k can be modeled by GMM model

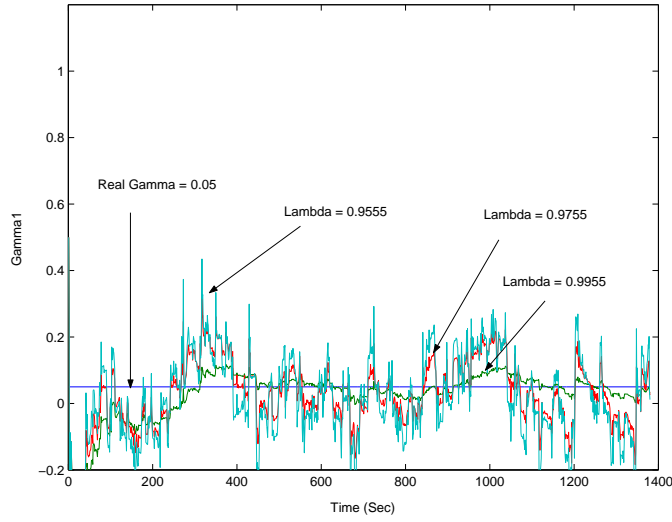


Figure 5.1: Parameter Estimation with different λ

as:

$$\alpha_k = 0.05\alpha_{k-1} + 0.95\bar{\alpha} + \sqrt{0.9975}X_{\alpha_{k-1}} \quad (5.1)$$

where initial value of $\bar{\alpha}$ is equal to 0° ; The MN varies $\bar{\alpha}$ to 30° at time instant 460 and 70° at time instant 920. $X_{\alpha_{k-1}}$ is a Gaussian random variable with zero mean and variance 10. Fig. 5.1 shows the parameter estimation of γ_1 using RLS with three different λ .

The speed of RWM model is switched between longer linear motion and shorter Brownian motion. The v_k can be modeled by linear motion of GMM model as:

$$v_k = 0.8v_{k-1} + 0.2\bar{V} + \sqrt{0.36}X_{V_{k-1}} \quad (5.2)$$

or Brownian motion of GMM model as:

$$v_k = 0.2v_{k-1} + 0.8\bar{V} + \sqrt{0.96}X_{V_{k-1}} \quad (5.3)$$

where the initial v_k is linear motion; The v_k changes to Brownian motion at time instant 400 and 860 with duration 60; The v_k returns to linear motion at time instant 460 and 920. $X_{V_{k-1}}$

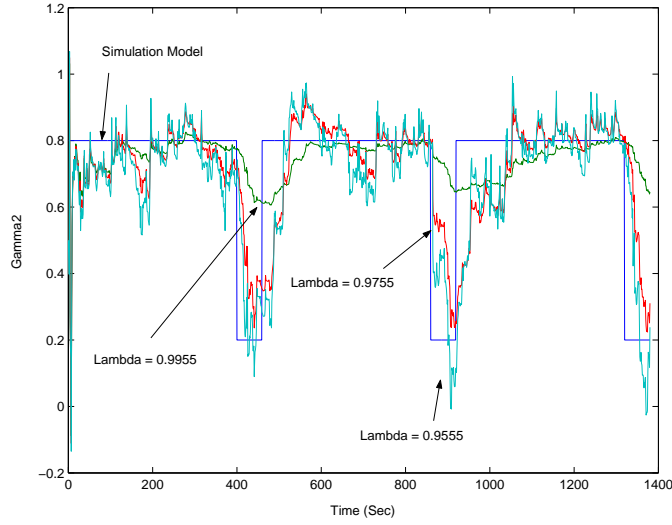


Figure 5.2: Parameter Estimation with different λ

is a Gaussian random variable with zero mean and variance 2. As shown in Fig. 5.2, the selection of λ to be 0.9955 results in the small variance of γ_1 but the convergence rate is too slow to follow the switched γ_1 . In order to follow the change of γ_1 with acceptable variance, the parameter λ is determined to be 0.9755.

5.1.2 Parameter Estimation of RWM Model under Different Simulation Models

In this section, the RLS algorithm are applied to three simulation models which represent the different level of randomness. The simulation models of heading angle α_k can be formulated as:

$$\alpha_k = 0.2\alpha_{k-1} + 0.8\bar{\alpha} + \sqrt{0.96}X_{\alpha_{k-1}} \quad (5.4)$$

$$\alpha_k = 0.1\alpha_{k-1} + 0.9\bar{\alpha} + \sqrt{0.99}X_{\alpha_{k-1}} \quad (5.5)$$

$$\alpha_k = \bar{\alpha} + X_{\alpha_{k-1}} \quad (5.6)$$

where the change of $\bar{\alpha}$ and random term are the same as mentioned in section 5.1.1. In Fig. 5.3, three heading angle with $\gamma = 0, 0.1, 0.2$ are estimated by RLS with $\lambda = 0.9755$.

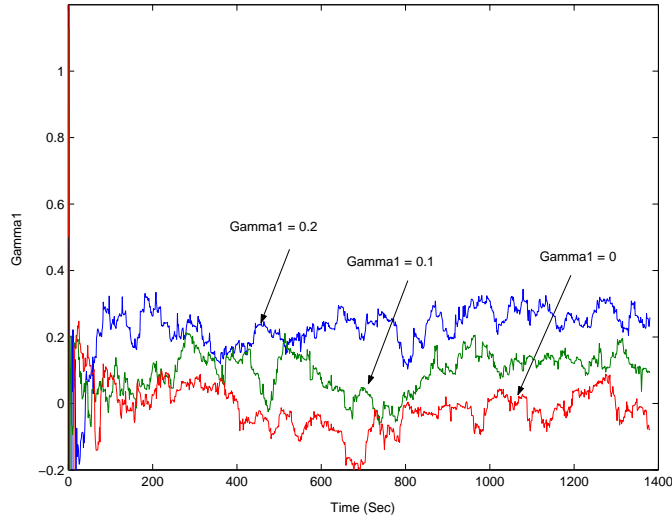


Figure 5.3: Parameter Estimation under different simulation models

The simulation models of speed v_k can be formulated as Table 1. The change of \bar{V} and random term are the same as mentioned in section 5.1.1. In Fig. 5.4, the parameters of three simulation models are estimated by RLS with $\lambda = 0.9755$. It can be shown that $\lambda = 0.9755$ can be chosen as our parameter under different simulation model.

TABLE 1

SIMULATION MODELS

SM1	$v_k = 0.9v_{k-1} + 0.1\bar{V} + \sqrt{0.19}X_{V_{k-1}}$ (Linear)
	$v_k = 0.1v_{k-1} + 0.9\bar{V} + \sqrt{0.99}X_{V_{k-1}}$ (Random)
SM2	$v_k = 0.8v_{k-1} + 0.2\bar{V} + \sqrt{0.36}X_{V_{k-1}}$ (Linear)
	$v_k = 0.2v_{k-1} + 0.8\bar{V} + \sqrt{0.96}X_{V_{k-1}}$ (Random)
SM2	$v_k = 0.7v_{k-1} + 0.3\bar{V} + \sqrt{0.51}X_{V_{k-1}}$ (Linear)
	$v_k = 0.3v_{k-1} + 0.7\bar{V} + \sqrt{0.91}X_{V_{k-1}}$ (Random)

5.1.3 Parameter Estimation of HM Model

The heading angle of HM model always moves toward one specified direction (i.e. $\bar{\alpha}$ is constant). The following equation represents the motion behavior of heading angle α_k using

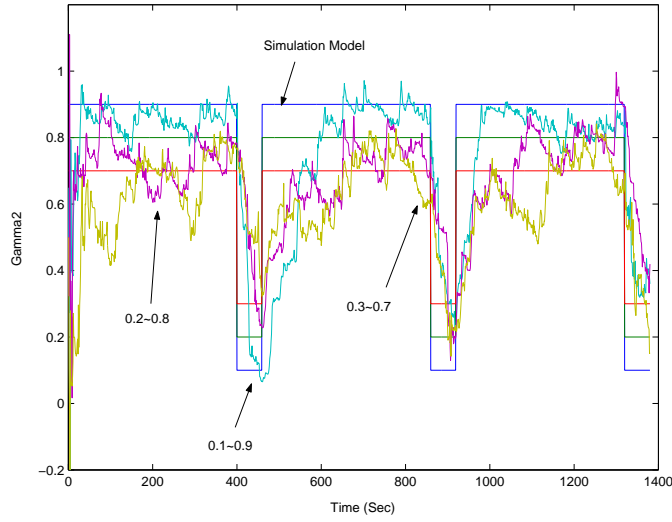


Figure 5.4: Parameter Estimation under different simulation models

GMM model:

$$\alpha_k = 0.5\alpha_{k-1} + \sqrt{0.75}X_{\alpha_{k-1}} \quad (5.7)$$

where $\bar{\alpha}$ points to zero degree and $X_{\alpha_{k-1}}$ is a Gaussian random variable with zero mean and variance 2. In Fig .5.5, three different λ (i.e. 0.9999, 0.999, and 0.99) is utilized in RLS and 0.9999 is chosen as our parameter due to the smallest variance.

The speed v_k of HM model mainly depends on the previous step v_{k-1} and the mean speed \bar{V} is changed when the MN moves to another lane. The speed v_k can be formulated by GMM model as:

$$v_k = 0.8v_{k-1} + 0.2\bar{V} + \sqrt{0.36}X_{V_{k-1}} \quad (5.8)$$

where the initial value of \bar{V} is 10m/s; \bar{V} varies to 15m/s at time instant 460, and 10m/s at time instant 920. $X_{V_{k-1}}$ is a gaussian random variable with zero mean and variance 2. In Fig 5.6, the parameter of speed v_k is estimated by RLS with three different λ (i.e. 0.9999, 0.999, and 0.99) and 0.9999 is chosen as our parameter due to the smallest variance.

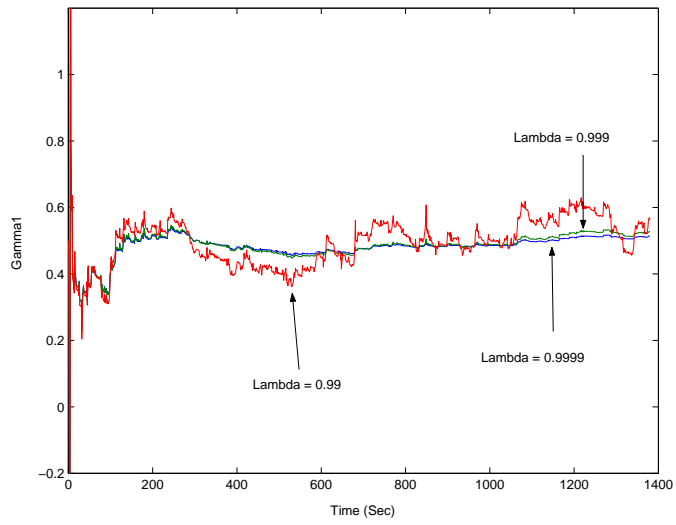


Figure 5.5: Parameter Estimation with different λ

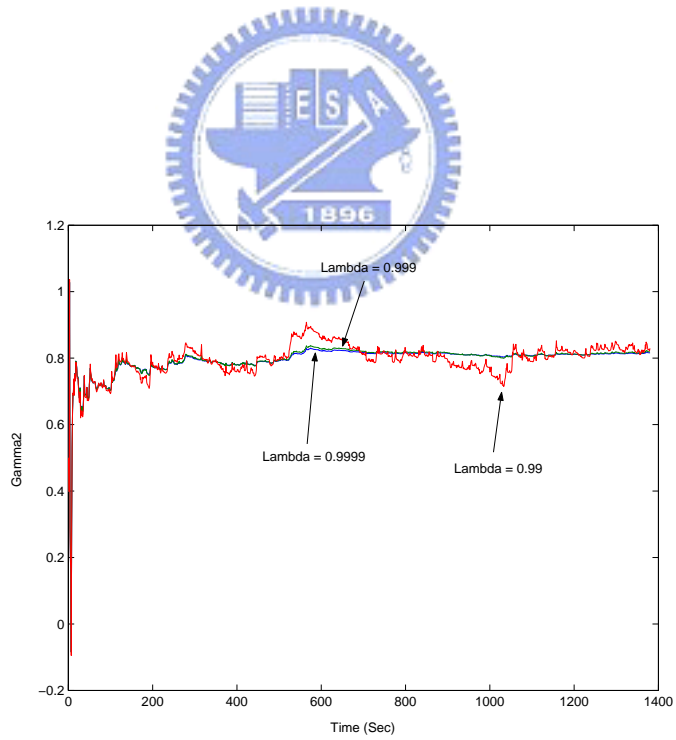


Figure 5.6: Parameter Estimation with different λ

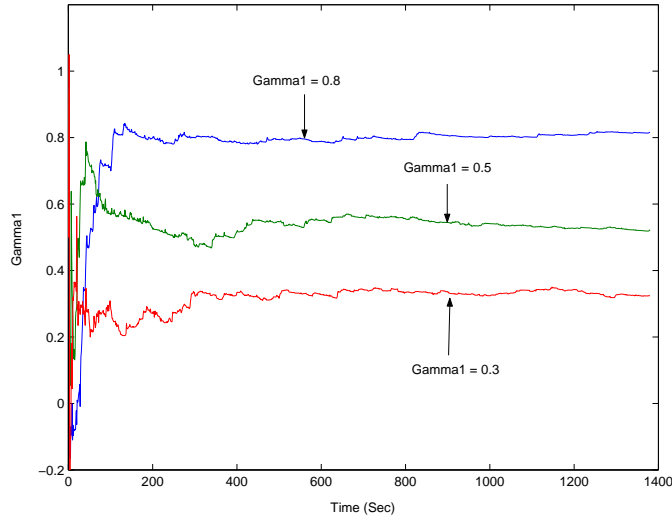


Figure 5.7: Parameter Estimation under different simulation model

5.1.4 Parameter Estimation of HM Model under Different Simulation Models

In order to present different levels of randomness, three simulation models are simulated using RLS. The heading angle α_k of different simulation model can be formulated by GMM model as:

$$\alpha_k = 0.8\alpha_{k-1} + \sqrt{0.36}X_{\alpha_{k-1}} \quad (5.9)$$

$$\alpha_k = 0.5\alpha_{k-1} + \sqrt{0.75}X_{\alpha_{k-1}} \quad (5.10)$$

$$\alpha_k = 0.3\alpha_{k-1} + \sqrt{0.91}X_{\alpha_{k-1}} \quad (5.11)$$

where the value of $\bar{\alpha}$ and $X_{\alpha_{k-1}}$ are defined in section 5.1.3. As shown in Fig. 5.7, three parameters are estimated by RLS with $\lambda = 0.9999$ which is determined from section 5.1.3.

The following equations represent the speed v_k of HM model with different level of randomness:

$$v_k = 0.8v_{k-1} + 0.2\bar{V} + \sqrt{0.36}X_{V_{k-1}} \quad (5.12)$$

$$v_k = 0.7v_{k-1} + 0.3\bar{V} + \sqrt{0.51}X_{V_{k-1}} \quad (5.13)$$

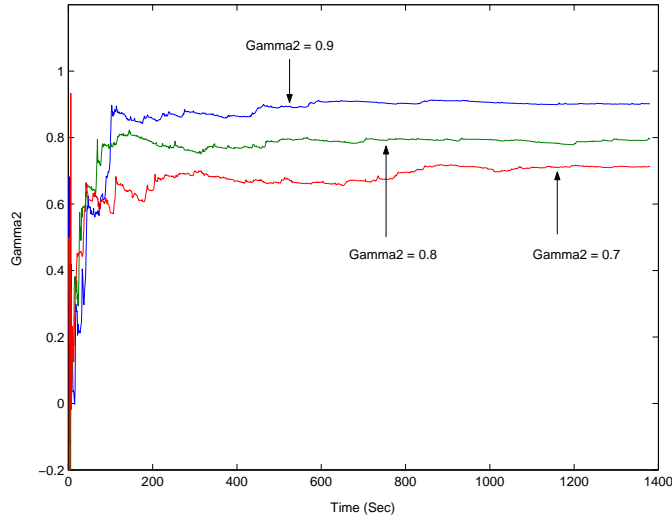
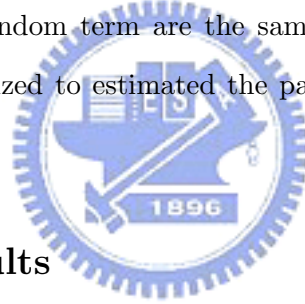


Figure 5.8: Parameter Estimation under different simulation model

$$v_k = 0.6v_{k-1} + 0.4\bar{V} + \sqrt{0.64}X_{V_{k-1}} \quad (5.14)$$

where the change of \bar{V} and random term are the same as mentioned in section 5.1.3. As shown in Fig. 5.8, RLS is utilized to estimate the parameters of simulation models using $\lambda = 0.9999$.



5.2 Simulation Results

5.2.1 Simulation Parameters

The simulations were conducted using the Network Simulator (ns-2, [37]) to compare the proposed VAR, PMLAR, and PMLAR-V algorithms with the existing LAR-Box and DSR protocols. In order to validate the effectiveness of the proposed algorithms, RWM and HM models are utilized in the simulations with their parameters as listed below:

- Random Waypoint Mobility Model: The RWM model is adapted within the simulation area of $500 \times 500 m^2$. The MNs' average pause time is set at 10 seconds.
- Highway Mobility Model: The HM model is adapted with four straight lanes (two lanes in each direction), each with 1 km in length and 4 m in width. The average speed of

the MNs in the fast lanes is 4 *m/sec* greater than that in the slow lanes. The variance of $X_{\alpha_{k-1}}$ for each MN is chosen to be 3°.

there are 70 MNs in RWM and 120 MNs in HM with 10 Constant Bit Rate (CBR) connections in the simulations. Each simulation runs for 600 seconds with the average speeds of the MNs at 5, 10, 15, 20 *m/sec*.

5.2.2 Simulation Results of the VAR Protocol

The results show the performance difference of the proposed VAR algorithm using GMM and CSM models. As shown in Fig. 5.9, 5.10, and 5.11, the VAR-GMM algorithm outperforms VAR-CSM algorithm in the RWM model. The data packet delivery ratio of VAR-GMM is 2 ~ 3% higher than the VAR-CSM; The end-to-end delay and the control packet load of VAR-GMM is smaller than the VAR-CSM. The more accurate predicting model are used, the batter performance can be obtained. The similar conclusions are also obtained in the HM model as shown in Fig. 5.9, 5.10, and 5.11. In the HM model, the MNs are arranged in a line and the VAR algorithm is easier to choose the route with batter quality. However, this arrangement may cause unreachable route if one of the intermediate MNs leaves the line. In the criterions in Eqn (4.4) and (4.5), $\delta_{1i} = 0.125$, $\delta_{2i} = 0.5$, $\delta_{1j} = 0.25$, and $\delta_{2j} = 0.5$ limit the broadcast of MNs.

5.2.3 Simulation Results of the PMLAR Protocol

This section compares the performance of proposed VAR, PMLAR, PMLAR-V with the existing DSR and LAR-Box protocols. By combining the PMLAR and VAR algorithms, the PMLAR-V have the best performance as shown in Fig. 5.12, 5.13, and 5.14. The VAR algorithm can improve the end to end delay of the protocol; However, the unnecessary MNs may be chosen as forwarding node, which increases the control packet load of protocol. In order to eliminate these nodes the LAR and PMLAR can be taken into consideration. It is noted that the LAR can be regard as the a spacial case of PMLAR when $\gamma_i = 1$; Therefore, the PMLAR have better performance than LAR protocol. Fig. 5.15, 5.16, and 5.17 show the

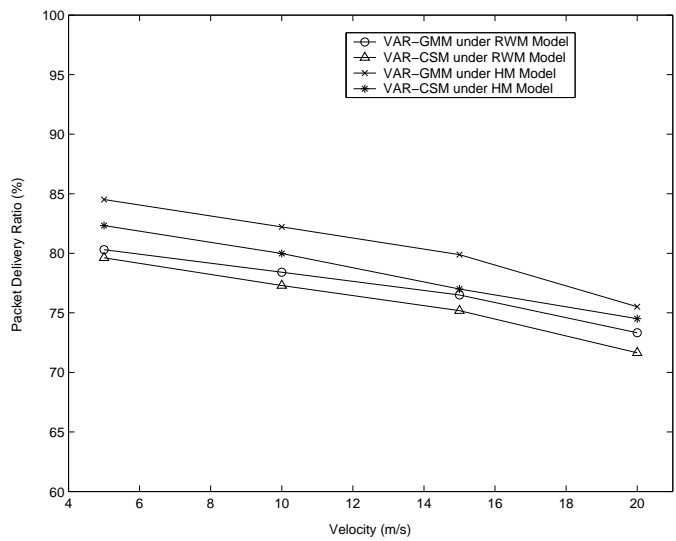


Figure 5.9: Data Packet Delivery Ratio with Random Waypoint and Highway Mobility Model

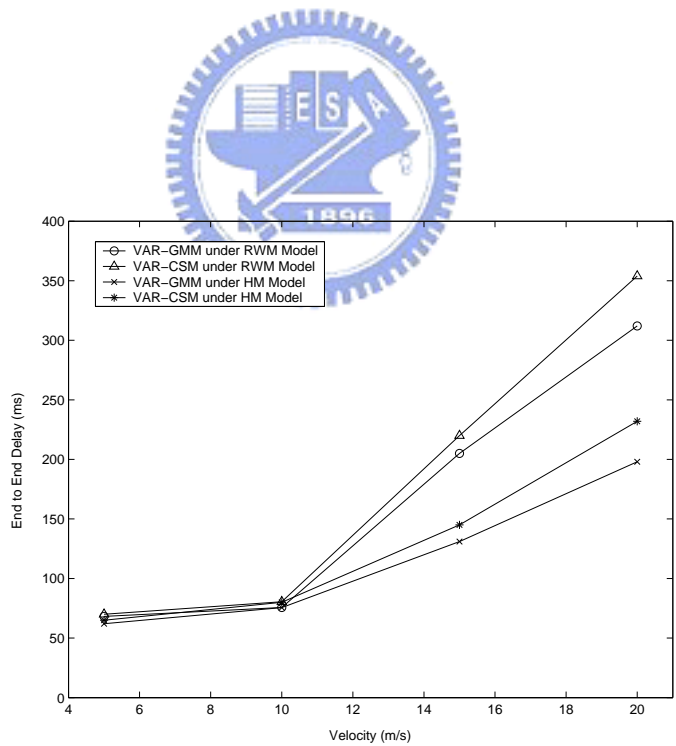


Figure 5.10: End to End Delay with Random Waypoint and Highway Mobility Model

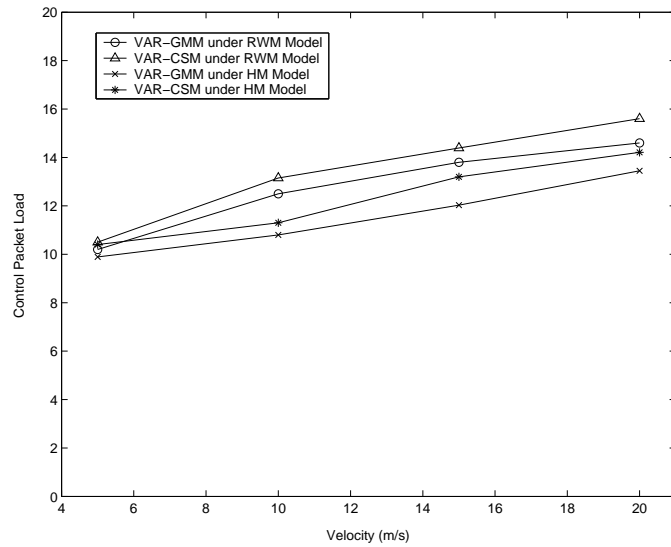
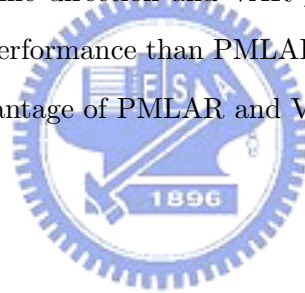


Figure 5.11: Control Packet Load with Random Waypoint and Highway Mobility Model

simulation results under highway mobility model. In highway mobility model, each MN has similar heading angle in the same direction and VAR protocol is suitable for this scenario. The VAR protocol has better performance than PMLAR except for control packet load. The proposed PMLAR-V takes advantage of PMLAR and VAR to obtain the best performance.



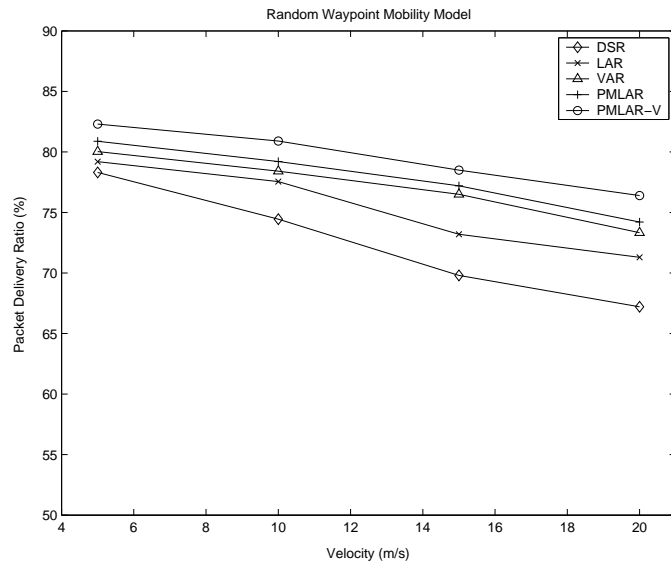


Figure 5.12: Data Packet Delivery Ratio with Random Waypoint Mobility Model

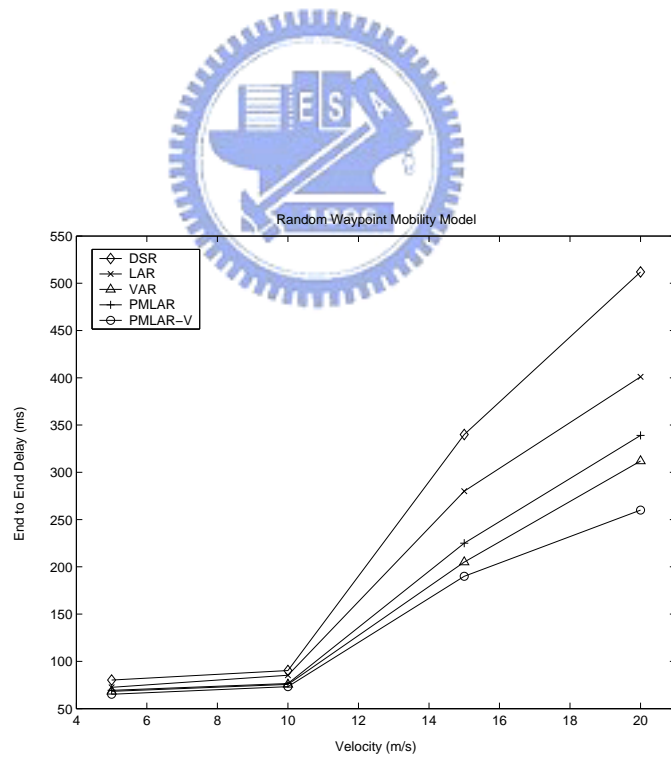


Figure 5.13: End to End Delay with Random Waypoint Mobility Model

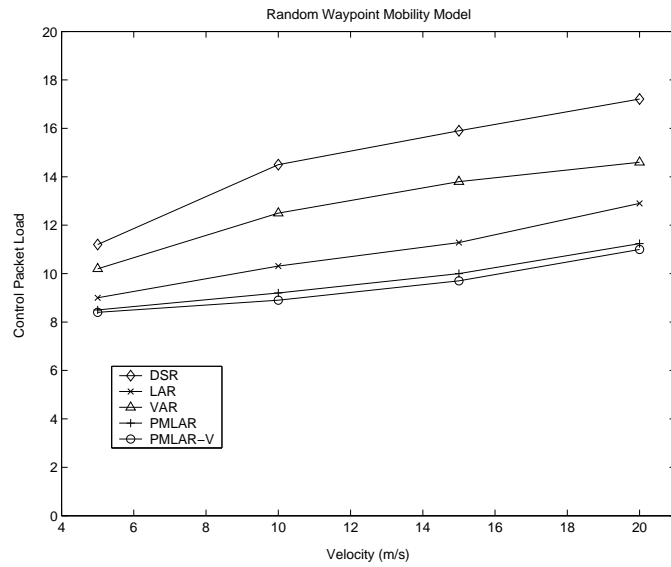


Figure 5.14: Control Packet Load with Random Waypoint Mobility Model

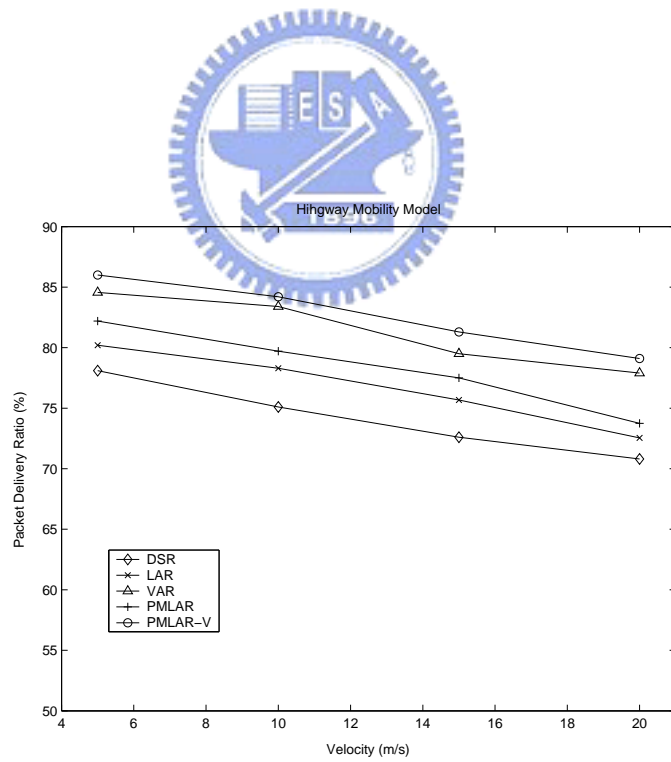


Figure 5.15: Data Packet Delivery Ratio with Highway Mobility Model

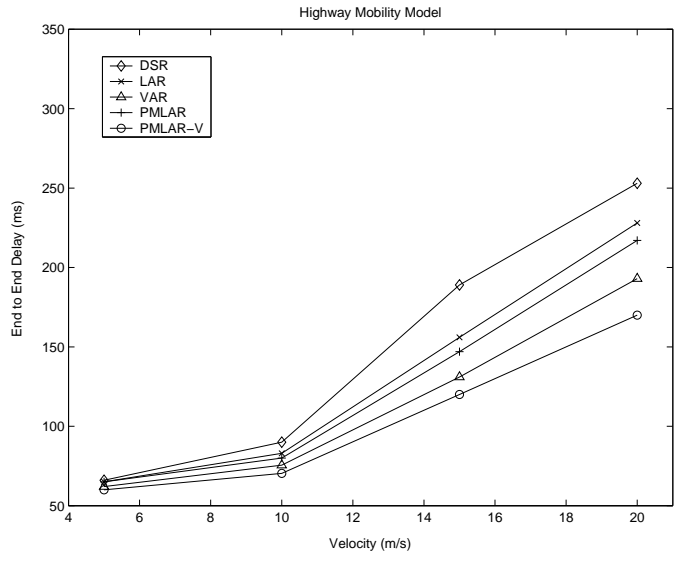


Figure 5.16: End to End Delay with Highway Mobility Model

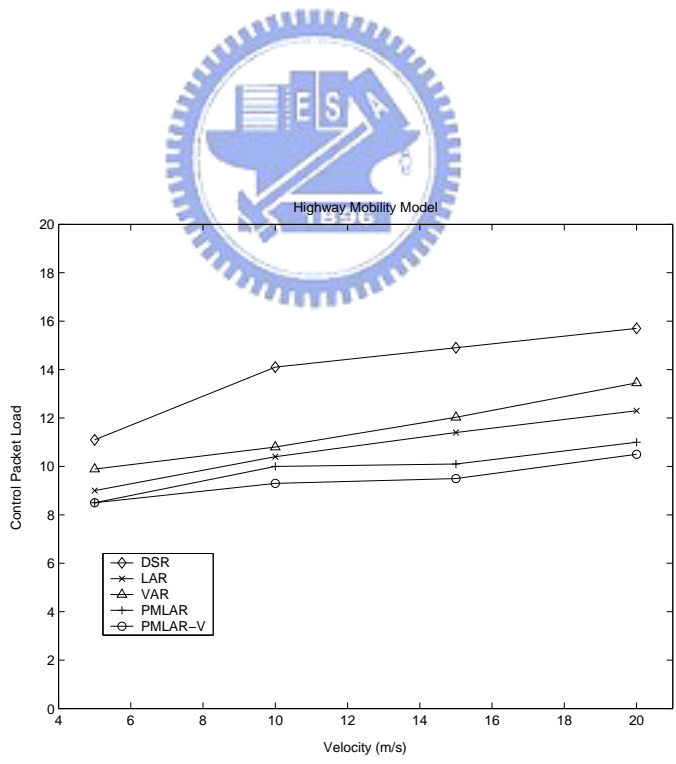
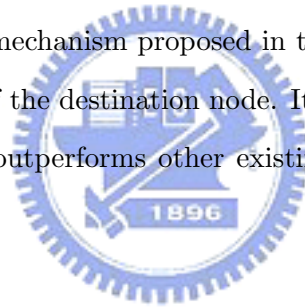


Figure 5.17: Control Packet Load with Highway Mobility Model

Chapter 6

Conclusions

In this thesis, the Velocity Aided Routing (VAR) and the Predictive Mobility and Location-Aware Routing (PMLAR) protocol are presented. By incorporating the mobility characteristics in the protocol design, the routing performance can be improved and adapted to different environments. The prediction mechanism proposed in the PMLAR algorithm can effectively forecast the future trajectory of the destination node. It is shown in the simulations that the proposed PMLAR-V protocol outperforms other existing protocols under different network topologies.



Bibliography

- [1] <http://www.isi.edu/nsnam/ns/ns-documentation.html>
- [2] Wireless LAN medium access control (MAC) and physical layer (PHY) specifications, IEEE standard 802.11, <http://www.ieee.org>
- [3] C. E. Perkins, and P. Bhagwat, "Highly Dynamic Destination Sequence Distance Vector (DSDV) Routing for Mobile Computers," *Proceedings of the ACM SIGCOMM '94 Conference*, August 1994, pp.234-244.
- [4] S. Murthy and J. J. Garcia-Luna-Aceves, "An Efficient Routing Protocol for Wireless Networks," *ACM Mobile Networks Appl. J., Special Issue on Routing in Mobile Communication Networks*, Oct. 1996, pp. 183-197.
- [5] C. Perkins, and E. Royer, "Ad-hoc On-demand Distance Vector Routing," *Proc. of the 2nd IEEE Workshop on Mobile Computing Systems and Applications*, February 1999, pp.90-100.
- [6] D. B. Johnson, D. A. Maltz, and J. Broch, "DSR: The Dynamic Source Routing Protocol for Multi-Hop Wireless Ad Hoc Networks," *Ad Hoc Networking*, edited by C. E. Perkins, Addison-Wesley, 2001.
- [7] V. D. Park and M. S. Corson, "A Highly Adaptive Distributed Routing Algorithm for Mobile Wireless Networks," *Proceedings of IEEE Infocom '97*, Apr. 1997, pp. 1405-1413.

- [8] C.-K. Toh, "A novel Distributed Routing Protocol to Support Ad-hoc Mobile Computing", *Proceedings of 15th IEEE Annual International Phoenix Conference on Computers and Communications*, March 1996, pp. 480-486.
- [9] R. Dube, C. D. Rais, K.-Y. Wang, and S. K. Tripathi, "Signal Stability Based Adaptive Routing (SSA) for Ad-hoc Mobile Networks," *IEEE Personal Communications*, Feb. 1997, pp. 36-45.
- [10] Z. J. Haas and M. R. Pearlman, "The Performance of Query Control Schemes for the Zone Routing Protocol," *IEEE/ACM Trans. Networking*, vol.9, no.4, Aug. 2001, pp.427-438.
- [11] P. Samar, M. R. Pearlman, and Z. J. Haas, "Hybrid Routing: The Pursuit of an Adaptable and Scalable Routing Framework for Ad Hoc Networks," in *The Handbook of Ad Hoc Wireless Networks*, Boca Raton, FL: CRC Press, 2003.
- [12] C.-C. Chiang, H. K. Wu, W. Liu, and M. Gerla, "Routing in Clustered Multihop, Mobile Wireless Networks with Fading Channel," *Proceedings of IEEE SICON '97*, Apr. 1997, pp. 197-211.
- [13] A. Iwata, C.-C. Chiang, G. Pei, M. Gerla, and T. W. Chen, "Scalable Routing Strategies for Ad Hoc Wireless Networks," *IEEE Journal on Selected Areas in Communication*, vol.17, no.8, Aug. 1999, pp. 1369-1379.
- [14] R. Sivahumar, P. Sinha, and V. Bharghavan, "CEDAR: a Core-Extraction Distributed Ad hoc Routing Algorithm," *IEEE Journal on Selected Areas in Communication*, vol.17, no.8, Aug. 1999, pp.1454-1465.
- [15] J. Borch, D. Maltz, D. Johnson, Y. Hu, and J. Jetcheva, "A Performance Comparison of Multi-Hop Wireless Ad Hoc Network Routing Protocols," *Proceedings of the ACM/IEEE International Conference on Mobile Computing and Networking*, October 1998, pp.25-30.
- [16] P. Johansson, T. Larsson, N. Hedman, B. Mielczarek, and M. Degermark, "Routing Protocols for Mobile Ad-Hoc Networks - A Comparative Performance Analysis," *Proceed-*

- ings of the ACM/IEEE International Conference on Mobile Computing and Networking, August 1999, pp.195-206.
- [17] E. R. Royer and C.-K. Toh, "A Review of Current Routing Protocols for Ad-hoc Mobile Wireless Networks," *IEEE Personal Communication Magazine*, April 1999.
- [18] S. R. Das, R. Castaneda, J. Yan, and R. Sengupta, "Comparative Performance Evaluation of Routing Protocols for Mobile, Ad hoc Networks," *Proceedings of the International Conference on Computer Communications and Networks (ICCCN)*, 1998, pp.153-161.
- [19] Y.-C. Tseng, S.-L. Wu, W.-H. Liao, and C.-M. Chao, "Location Awareness in Ad Hoc Wireless Mobile Networks", *IEEE Computer*, June 2001, pp.46-52.
- [20] B. Parkinson and S. Gilbert, "NAVSTAR: Global Positioning System - Ten Years Later," *Proceedings of IEEE*, October 1983, pp.1177-1186.
- [21] S. Basagni, I. Chlamtac, V. R. Syrotiuk, and B. A. Woodward, "A Distance Routing Effect Algorithm for Mobility (DREAM)," *Proceedings of the ACM/IEEE International Conference on Mobile Computing and Networking*, October 1998, pp.76-84.
- [22] Y.-B. Ko and N. H. Vaidya, "Location-Aided Routing (LAR) in Mobile Ad Hoc Networks," *ACM Wireless Networks Journal*, vol.6, no.4, 2000, pp.307-321.
- [23] R. Jain, A. Puri, and R. Sengupta, "Geographical Routing using Partial Information for Wireless Ad Hoc Networks" *IEEE Personal Communications*, vol.8, no.1, 2001, pp.48-57.
- [24] B. Karp, and H. T. Kung, "GPSR: Greedy Perimeter Stateless Routing for Wireless Networks," *Proceedings of the ACM/IEEE International Conference on Mobile Computing and Networking*, August 2000, pp.243-254
- [25] J. Li, J. Jannotti, D. S. J. De Couto, D. R. Karger, and R. Morris, "A Scalable Location Service for Geographic Ad Hoc Routing", *Proceedings of the ACM/IEEE MobiCom*, Aug. 2000, pp.120-130.

- [26] R. Morris, J. Jannotti, F. Kaashoek, J. Li, and D. S. J. De Couto, "Carnet: A Scalable Ad Hoc Wireless Network System," *Proceedings of the 9th ACM SIGOPS European Workshop: Beyond the PC: New Challenges for the Operating System*, Sep. 2000.
- [27] M. Mauve, J. Widmer, and H. Hartenstein, "A Survey on Position-Based Routing in Mobile Ad-Hoc Networks," *IEEE Network Magazine*, vol.15, no.6, November 2001, pp.30-39.
- [28] T. Camp, J. Boleng, B. Williams, L. Wilcox, and W. Navidi, "Performance Comparison of Two Location Based Routing Protocols for Ad Hoc Networks," *Proceedings of the IEEE 21st Annual Joint Conference of the IEEE Computer and Communications Societies (INFOCOM '02)*, 2002, pp.1678-1687.
- [29] P. Yao, E. Krohne, and T. Camp, "Performance Comparison of Geocast Routing Protocols for a MANET," *Proceedings of the 13th IEEE International Conference on Computer Communications and Networks (IC3N)*, 2004, pp.213-220.
- [30] G. Lin, G. Noubir, and R. Rajmohan, "Mobility Models for Ad Hoc Network Simulation," *INFOCOM 2004*, March, 2004.
- [31] D. Yu and H. Li, "Influence of Mobility Models on Node Distribution in Ad Hoc Networks," *Proceedings of ICCT 2003*, 2003, pp.985-989.
- [32] T. Camp, J. Boleng, and V. Davies, "A Survey of Mobility Models for Ad Hoc Network Research," *Wireless Communication and Mobile Computing (WCMC): Special issue on Mobile Ad Hoc Networking: Research, Trends and Applications*, vol.2, no.5, 2002, pp.483-502.
- [33] D. Son, A. Helmy, B. Krishnamachari, "The Effect of Mobility-Induced Location Errors on Geographic Routing in Ad Hoc Networks: Analysis and Improvement using Mobility Prediction," *IEEE Transactions on Mobile Computing*, vol.3, no.3, 2004, pp.233-245.
- [34] A. Gelb, *Applied Optimal Estimation*, The M.I.T. Press, 1974.

- [35] B. Liang, and Z. Haas, "Predictive Distance-Based Mobility Management for PCS Networks," *Proceedings of the Joint Conference of the IEEE Computer and Communications Societies*, March 1999.
- [36] X. Hong, M. Gerla, G. Pei, and C. Chiang, "A Group Mobility Model for Ad Hoc Wireless Networks," *Proceedings of the ACM International Workshop on Modeling and Simulation of Wireless and Mobile Systems*, August 1999.
- [37] J. Heidemann, N. Bulusu, J. Elson, C. Intanagonwiwak, K. Lan, Y. Xu, W. Ye, D. Estrin, and R. Govindan, "Effects of Detail in Wireless Network Simulation," *Proceedings of the SCS Multiconference on Distributed Simulation*, January 2001, pp.3-11.
- [38] S. L. Jr. Marple, *Digital Spectral Analysis with Applications*, Prentice Hall, Englewood Cliffs, 1987.

